NASA

Technical Memorandum 79706

Energetic Protons in the Jovian Magnetosphere

F. B. Mc Donald, A. W. Schardt, and J. H. Trainor

JANUARY 1979

National Aeronautics and Space Administration

Goddard Space Flight Center
Greenbelt, Maryland 20771

Energetic Protons in the Jovian Magnetosphere

F. B. McDonald, A. W. Schardt, J. H. Trainor
Laboratory for High Energy Astrophysics
NASA/Goddard Space Flight Center
Greenbelt, Maryland 20771

Abstract

The time histories, angular distributions and energy spectra of energetic protons have been measured over an energy range extending from 0.2 - 20 MeV for the four passes of Pioneers 10 and 11 through the Jovian magnetosphere. The energetic particle data from these four passes are remarkably different. Azimuthal asymmetries appear to dominate with time variations also contributing to the very complex topology. On the inbound P-10 pass the expected corotation anisotropy was not observed in the outer magnetosphere supporting the probable existence of a planetary wind in this region. Near the dawn meredian particle streaming away from the planet begins at ~15 R_J. On both the P-10 inbound and P-11 outbound passes, there are regions where only partial corotation is achieved. In the mid-magnetosphere, field-aligned streaming away from the near-equatorial current sheet region is the most prominent and puzzling feature. At mid-latitudes in the subsolar regime, the streaming pattern is more chaotic and its magnitude is smaller. Qualitative discussions are presented for a number of possible mechanisms which could produce this streaming. In the context of our present understanding of the Jovian magnetosphere, each of three mechanisms show promise: perpendicular electric fields, a strong azimuthal intensity gradient at the equator, and strong diffusion processes. In the Jovian wind regions, proton energy spectra are generally of the form $E^{-\gamma}$ where E is the kinetic energy of the particle with γ generally ranging between values of 3.0 and 4.2. For the remaining times, the spectra are most frequently of the form $\exp -P/P_o$ where P is the proton momentum with P_o varying mainly between 8.0 and 12 MV.

I. INTRODUCTION

The passage of Pioneers 10 and 11 by the planet Jupiter has revealed a large, dynamic and complex magnetosphere which differs in many important aspects from that of the Earth. An excellent summary of the data from the energetic particle, magnetic field and plasma experiments is contained in the review paper of Kennel and Coroniti (1977). The synthesis of these results have revealed at least three distinct regions:

1. The outer magnetosphere which extends from $\sim$50 to $\sim$100 R_J. In this region neither the particle fluxes nor the magnetic field show strong radial dependence. There is a large regular 10 hour variation in the >5 MeV electron intensity which is absent for the low energy electron and proton component. Time variations, which may be produced either by changes in the solar wind pressure or asymmetries in the evolution of plasma (Dessler and Hill 1978), are very important. The observed magnetic field is irregular and generally much larger than that predicted for a dipole field. The total energy carried by the energetic particles and plasmas appears to be of the same order as that of the Jovian magnetic field.

2. The middle magnetosphere extends from $\sim$15 R_J to $\sim$50 R_J. In this region the Jovian magnetic field is distorted by the presence of a plasma sheet close to the equatorial plane. The magnetic field increases with decreasing radial distance. The electron intensity also increases while the proton intensity remains essentially constant. The energy of the magnetic field dominates over that of the energetic particles and plasma.

3. The inner magnetosphere inside $\sim$15 R_J corresponds more closely to the Earth's trapped radiation region with the added complexity of the enormous effects of the Galilean satellites.

This tentative morphology is a somewhat arbitrary but useful even though the boundaries between regions are not well defined. Very important portions of the Jovian magnetosphere, such as the tail and dusk regions, have yet to be explored. Furthermore, the existing data suggest that azimuthal variations are very important.

Energetic particles are a useful tool for exploring and defining the properties of these different magnetospheric regions. In this paper the emphasis is on the study of the energy spectra and angular distribution of the ion-component from the bow-shock to $\sim$15 R_J over an energy interval from 0.2 to 20 MeV. The region inside 15 R_J is very different from the outer portions and will not be discussed in this paper.

The systematic study of energy spectra and angular distributions of magnetospheric ions are of fundamental importance in understanding their acceleration, transport and loss processes. For example, in the outer zone of the Earth's magnetosphere, the energy spectra and angular distribution both become progressively flatter with decreasing distance as would be expected from radial diffusion. In the tail region and the flanks of the magnetosheath, uni-directional streaming of ions and electrons is observed and it is generally assumed that these particles are accelerated by field-line merging.

In the present study it is found that between the magnetopause and 15 R_J the measured proton angular distributions in the Jovian magnetosphere are dominated by large first-order anisotropies. These first-order anisotropies are produced by a combination of field-aligned streaming, corotation effects with a much smaller contribution from spatial gradients in the particle intensity. Due to the large scale of the Jovian magnetosphere and the rapid rotation of the planet, it was expected that the corotation anisotropy would dominate. For example the expected corotation anisotropy just inside the magnetopause at 100 R_J for 0.5 MeV protons (assuming an energy spectra of E^{-4}) is 80%. For the Earth's magnetosphere, the effect is ~250 times smaller or ~0.3%. Conversely, the measured anisotropy can be used to test whether or not the particles are rotating with the planet. On the in-bound pass of Pioneer 10 (P-10-in) between 95 and 70 R_J, corotation was not observed. This result is most readily interpreted in terms of a Jovian wind. The mid-magnetospheric region as observed with both the Pioneer 10 and 11 inbound passes is dominated by field-aligned streaming. In the "Jovian-wind" region particle energy spectra are generally of the form $E^{-\gamma}$ where E is the kinetic energy. For the remaining times, the spectra are most frequently of the form exp - P/P_o where P is the proton momentum. Curiously, there is almost a complete absence of systematic changes of P_o with radial distance between 100 and 20 R_J; however, in the mid-magnetosphere there appears to be a dependence on distance from the magnetic equator

The large field aligned anisotropy and the nearly constant equatorial proton intensities and spectra between 25 and 64 R_J suggest that the

mid-magnetosphere is not a classical trapping region and the ions appear to have a lifetime of at most a few hours. Detailed comparisons of the particle intensity at different energies for 2 in-bound and out-bound trajectories suggest the outer regions represent complex combination of temporal changes and azimuthal variations.

II. TRAJECTORY INFORMATION

The Pioneer 10 and 11 trajectories relative to Jupiter are shown in Fig. 1. As viewed in local Jovian time, Pioneer 10 was on a prograde trajectory which approached Jupiter from a direction approximately 35^{o} west of the sun at 100 R_J, circled the planet in a counter-clockwise direction and exited toward the dawn meredian. The initial approach trajectory of Pioneer 11 was some 43^{o} west of the Jovian-sun line and the in-bound trajectory was very similar to that of Pioneer 10 through the outer and mid-magnetosphere. However, Pioneer 11 circled the planet in a clockwise direction and exited at moderately high northern latitudes ($30-50^{o}$) close to the noon meredian. Both P-10-in and P-11-in sampled low, southerly Jovigraphic latitudes near 1000 local time. Pioneer 10 out-bound (P-10-out) was at a low latitude (10^{o}) in the northern hemisphere near the dawn meredian.

III. OVERVIEW OF THE PIONEER 10 and 11 TRAVERSALS OF THE JOVIAN MAGNETOSPHERE

Investigators of the four energetic particle experiments on Pioneer have published detailed views of the mid and outer Jovian magnetospheres which are remarkably consistent (Filius 1976, McDonald and Trainor 1976, Simpson and McKibben 1976, Van Allen 1976). In this section the 0.2 - 0.5 MeV LET II proton data along with the 1.1-1.6 LET I proton measurements (Trainor et al., 1974) are used to directly inter-compare the

4 passages through the Jovian magnetosphere. Because of the importance of 10 hour variations, the data have been plotted on a linear time scale rather than as a function of radial distance. Significant distortions are not introduced by this choice since the spacecraft velocity in the outer and mid-magnetosphere was essentially the same at a given radial distance for all passes. The proton intensities for Pioneer 10 and 11 in-bound (P-10-in, P-11-in) are shown in Figure 2 for the two different energy values. The initial encounters with the bowshock and magnetopause occurred at the same radial distance within a few R_J for both spacecraft (Intriligator and Wolfe, 1976). However, Pioneer 10 remained inside the magnetosphere for 3 days while Pioneer 11 crossed the bow shock at 109.7, 91.6 and 77.5 R_J suggesting greater variability in the solar wind pressure. There appear to be no great differences in the low energy flux between Pioneer 10 and 11 from ~95 R_J to ~45 R_J except that on the average the Pioneer 10 intensity was somewhat higher. Thus the magnetopause apparently does not constitute a trapping boundary for protons below 0.5 MeV. As Simpson et al. (1976) have emphasized however, the magnetopause boundary appears to provide effective containment for the magnetospheric energetic particles above 0.5 MeV with an e-folding distance of 1-2 R_J. Thus we find a drop-out of 1.1-1.6 MeV protons (Fig. 2) whenever either of the spacecraft is in the magnetosheath.

The passages of Pioneer 10 and 11 through the mid-magnetospheres are dramatically different. Near 45 R_J both spacecraft measure approximately equal fluxes at the two energy levels. At smaller radial distances each observe a well-defined, approximate 10 hour periodicity with the respective flux maxima remaining essentially constant between ~20 and 40 R_J. However, the Pioneer 11 intensities are approximately

a factor of 20 lower than those of Pioneer 10, and in fact, the Pioneer 11 intensity maxima lie close to or below the adjacent Pioneer 10 minima. Furthermore, the intensities of these minima increase with decreasing distance on Pioneer 10 but display exactly the opposite behavior on Pioneer 11. It is expected that the rotation of the offset dipole produces a vertical displacement of a magnetic field line relative to the magnetic equator of $\sim 8\ R_J$ between 30 and 40 R_J. In this region the actual Pioneer 11 orbit is $\sim 1.5\ R_J$ below that of Pioneer 10. This displacement is much too small to produce the two orders of magnitude difference observed between Pioneer 10 and 11 at 32 R_J.

Figure 3 shows the flux of 0.2-0.5 MeV protons between 15 and 150 R_J for P-10-out. All observers have noted both the dominance of the 10 hour variations with the intensity minima approaching the background level of the various detector systems and the highly variable position of the magnetopause. Near the magnetopause the 10 hour periodicity essentially disappears. As previously suggested by Simpson and McKibben (1976), the intensity variations observed by P-11-in, between 40 and 15 R_J, resembles the corresponding observations on P-10-out toward the dawn meredian. Superimposing the particle data for the two passes show (Fig. 3) reasonable agreement over the inner portion of the mid-magnetosphere. However, at larger radial distances the relative behavior becomes very disparate.

Figure 4 compares the P-10-in data with the mid-latitude data from P-11-out. The P-11-out data display no obvious 10 hour periodicities and the average mid-magnetosphere intensity is much smaller than on

the P-10 inbound leg. Between 35 and 55 R_J, P-10-in was between -16 and +5° magnetic latitude while P-11-out was between +23 to +44°. To the extent that the particle population is symmetrical relative to the magnetic equator and is also azimuthally symmetric, P-11-out data provide an extention to higher latitudes. Thus the peak P-11-out flux is only slightly less than the minimum P-10-in flux between 15 and 45 R_J. Between 45 and 82 R_J the 0.2-0.5 intensities generally agree within a factor of 2. The P-11-out intensities are generally of the same order as observed on P-11-in.

IV. ENERGY SPECTRA

Differential energy spectra (0.2-21 MeV) of the ion component are obtained from two separate detector systems with very different geometric factors and alpha and electron response functions (Trainor et al. 1974). The integral energy thresholds along with the derived differential intervals are listed in Tables I and II for both detectors. The agreement between the fluxes determined from the LET I and LET II systems is excellent. This good agreement is a further indication that the low energy spectra are not significantly distorted by the helium component. At energies above 3.3 MeV/nuc multiparameter analysis provides complete separation of the two components. For P-10-in, the energy spectra can generally be represented as a power-law in kinetic energy, $E^{-\gamma}$, from 100 R_J to 60 R_J (Fig. 5). Note the complex spectra observed at 76.8 R_J where a well-defined "flat-region" develops between 0.8 and 2 MeV. This form appears at irregular intervals throughout the Jovian magnetosphere and can persist for 2-3 hours. At smaller radial distances the data can no longer be described by a single power-law in kinetic energy (Fig. 5). However, over most of the region inside

60 R_J, the spectra can be represented by the form $dJ/dp = C \exp -P/P_o$ (Fig. 6) where P is the proton momentum. For the other three passes an acceptable fit with an exponential in momentum was obtained for 80-90% of the hourly averages inside the magnetosphere after eliminating those periods when the counting rates were too low to make a meaningful determination. On P-10-out, there are also several periods including the time just inside the first magnetopause crossing when spectra of the form $E^{-\gamma}$ are obtained. In all 4 data sets there were hourly intervals with low intensity and steep spectra (small P_o or large γ) when it is not possible to distinguish between an exponential in momentum or a power law in kinetic energy.

The spectral characteristics for the 4 passes can now be examined in terms of the variation of P_o with radial distance (Fig. 7, 8, 9). For P-10-in and P-10-out the radial variation of γ is also included for those periods when a $E^{-\gamma}$ spectra are applicable. The unmarked arrows in the three figures mark the occurrence of well defined intensity maxima occurring inside the magnetopause. For P-10-in (Fig. 7) there is a correlation between these intensity peaks and increases in P_o especially at $\sim$41 and 36 R_J where large increases in P_o occur (from $\sim$9 MV to >14 MV). Except for these two peaks, P_o shows a remarkably small variation with an average value of 9 - 10 MV over the complete in-bound traversal of the outer and mid-magnetosphere by Pioneer 10. Similarly, γ displays almost no variation between 100 and 60 R_J. Note, however, that in the inner magnetosphere P_o increases very rapidly

with decreasing radial distance. This sharp increase is probably the best signature currently available for defining the boundary between the inner and mid-magnetospheres.

Pioneer 10-out (Fig. 8) shows a similar transition between 10 and 13 R_J. Beyond 13 R_J, P_o remains essentially constant at an average value of 7 MV with small increases of 1-2 MV associated with intensity maxima. Just prior to the first magnetopause crossing near 100 R_J, the spectra are either a power law in kinetic energy with $\gamma \sim 3$ or have P_o's $\sim$ 9-10 MV - indicating in either case enhanced fluxes of higher energy particles.

The plot of P_o (Fig. 9) for P-11-in between 64 and 4 R_J bears a strong resemblance to the intensity profile for this pass (Fig. 2). From 65 to 45 R_J, P_o varies between 10.5 and 8.7 MV. At smaller radial distances there are quasi-periodic decreases in P_o which tend to coincide with the intensity minima. Furthermore these minimum spectra become increasingly soft with decreasing radial distance in the same fashion that the particle intensity decreased. There is a rapid increase of P_o between 17 and 13 R_J from 5.4 to 17 MV with no further increase above 20 MV into 4 R_J. During this period the spacecraft is generally at Jovian magnetic latitudes above 45°N. P-11-out observes a very soft spectrum with an average value of $\sim$7 MV between 8 and 40 R_J which increases to $\sim$10 MV between 40 and 60 R_J (Fig. 9).

For all 4 passes through the Jovian outer and mid-magnetospheres there are essentially no systematic spectral changes with radial distance

except that P_o is generally somewhat larger just inside the magnetopause than at smaller radial distances in the mid-magnetosphere. Between 15 and 45 R_J, however, spectra are distinctly harder at the magnetic equator than about 8 R_J below or above it.

V. ANGULAR DISTRIBUTIONS

The LET II proton data is divided into eight 45^o sectors for three energy intervals

i. 0.5 - 2.2 MeV

ii. 1.2 - 2.2 MeV

iii. 1.8 (P-10) - 2.2 MeV

1.5 (P-11) - 2.2 MeV

The 2 lower energy levels were used in the present analysis because the narrow high energy channel was more subject to contamination of low energy helium nuclei. The analysis procedures for this experiment were developed by Zwickel and Webber (1976). The particle distribution $J(\theta)$ is expressed in terms of a Fourier series:

$$J(\theta) = A_o + \sum_{n=1}^{2} \{ a_n \cos(n\theta) + b_n \sin(n\theta) \} = A_o + \sum_{n=1}^{2} A_n \cos n(\theta - \theta_n)$$

and $\theta_n = \frac{1}{n} \tan^{-1} b_n/a_n$; $A_n/A_o = (a_n^2 + b_n^2) \div A_o$

with the n^{-th} order anisotropy being A_n/A_o.

The coefficients are determined by a least square fit to the observational data. If the actual A_1/A_o is directed at an angle β with respect to the scan plane, then it is necessary to divide $(A_1/A_o)_{obs}$ by cos β. Corrections for the finite opening angle of the detector increases the actual value of A_1/A_o by an additional 4%. These corrections are made for those cases when the measured anisotropy is compared with the values calculated for corotation. Zwickel and Webber (1976) also pointed

out that the measured anisotropy is generally greater than the true anisotropy due to statistical fluctuations. This effect is important when the statistical errors are large. The present analysis has been restricted to those periods when the observed anisotropy is more than twice as large as the calculated standard error.

A typical example of a 1 hour average of observed angular distributions is shown in figure 10. As seen from earth, angles are measured counter clockwise from the North which is taken to be perpendicular to the spin axis. θ_1 designates the direction of the first order anisotropy relative to North, and α_1 is its angle relative to the projection of the magnetic field, $\overline{B}$, into the scan plane. There are three principal physical processes that could play a role in producing these observed anisotropies (Trainor et al. 1974).

a. Corotation effects: If the observer moves relative to the rest frame of the plasma, the observed particles have a different energy and come from a different direction than in the rest frame. However, the particle distribution function in momentum space, f, is invariant under such a velocity transform with

$$\frac{J(E)}{E} = \frac{J(E')}{E'} = 2fm$$

where E and E' are the particle kinetic energy in the moving frame and the rest frame of the plasma, respectively, and m is the particle mass. The expected corotation anisotropy at a given energy is given by

$$\xi(E) = \frac{\frac{1}{E_2} J(E_2) - \frac{1}{E_1} J(E_1)}{\frac{1}{E_1} J(E_1) + \frac{1}{E_2} J(E_2)}$$

$E_1 = 1/2\ m(v + v_r)^2$ and $E_2 = 1/2\ m\ (v - v_r)^2$

v_r = corotation velocity and $\xi(E)$ is the anisotropy.

To a first approximation this can be written as

$$\xi(E) = 2\ (1 + \gamma)\ \frac{v_r}{v} \propto 2\ (1 + \gamma)\ \frac{v_r}{E^{\frac{1}{2}}},\quad E = \tfrac{1}{2}\ mv^2$$

which is the Compton-Getting effect. When γ, the spectral index $[J(E) \propto E^{-\gamma}]$ is constant with energy, this effect decreases with increasing kinetic energy. However, for an exponential in momentum, γ increases with E so the energy dependence is reduced. In practice, sectored measurements are based on two fixed energies, E_T and E_M, where E_T is the threshold energy for a given level and E_M = 2.2 MeV is the maximum energy. The calculated corotation anisotropy is obtained by integrating over the measured spectrum between E_T and E_M.

b. Gradient effects: The guiding centers of the observed particles are not at the satellite, but located on a circle one gyroradius away; thus an asymmetry perpendicular to the magnetic field is observed if a gradient exists in the particle population. This effect is especially important in the outer magnetosphere with its relatively weak magnetic field. For example in a 10 γ field, the gyroradius of a 2 MeV proton is 0.29 R_J and a doubling of the proton intensity per R_J can produce a 30% anisotropy. The gradient anisotropy ξ_g is given by

$$\xi_g(E) = \frac{R_g}{J}\ \frac{dJ}{dR}$$

where R_g is the gyroradius of protons of energy E. ξ_g increases as $E^{\frac{1}{2}}$ with increasing kinetic energy.

c. Field-aligned streaming: A number of physical processes which could produce this effect are covered in the discussion section.

Because of the direction of the Jovian magnetic field and its direction of rotation, the gradient and corotation anisotropies will be in the same direction for protons if the particle flux increases towards the planet. Both of these effects are much smaller for electrons than for ions and do not make a measurable contribution to the electron angular distributions.

The geometry of the spacecraft trajectory determines which processes can be observed. The LET II scans in a plane perpendicular to the spin axis of the spacecraft (Fig. 10) which in turn is directed at the Earth; except for P-10-out this direction is generally within 30° of being radially away from Jupiter (Fig. 1). Thus corotation and radial gradient anisotropies can be detected on P-10-in and P-11-in and P-11-out but not on P-10-out. In the latter case the direction of the corotation and gradient anisotropies coincide closely with the direction of the spacecraft spin axis. However, P-10-out is the only pass where energetic particles moving radially outward could be detected directly. It is important to keep in mind in studying first order anisotropies, that meaningful measurements can be made even during periods when the magnetic field is at a substantial angle with respect to the scan plane of the spacecraft because the effect decreases only as the cosine of that angle.

The superposition of the three different processes produced a variety of angular distributions. The distributions observed on P-10-in

between 15 and 45 R_J are well organized (Fig. 11). At the four flux maxima the magnetic field was generally pointed down corresponding to the anticipated plasma sheet configuration. The first order anisotropy was nearly perpendicular to $\overline{B}$ and pointed in the direction from which maximum flux would be expected due to corotation. At the flux minima the measured anisotropy was larger and almost aligned with the direction of the magnetic field.

The nature of these first-order anisotropies is clearer if one simultaneously examines their magnitude and direction (A_1/A_o and θ_1), the intensity level, and α_1 (the angle between θ_1 and the projection of the magnetic field in the scan plane of the spacecraft). These data are shown in four panels (Fig. 12) for 0.5-2.2 and 1.1-2.2 MeV protons for P-10-in. The generally very excellent agreement between values of θ_1 at two different energies adds confidence that the measurements are not distorted by fluctuations in the counting rate or by other effects. The distribution between 15 and 45 R_J vary in a systematic way between flux maxima and minima (with the angular distributions of Fig. 11 being the extremes), and A_1/A_o displaying a series of well-defined peaks which occur approximately every 10 hours. These peaks coincide with the counting rate minima and with values of α_1 between 140^o and 180^o. As McDonald and Trainor (1976) have shown previously, the directions of θ_1 and α_1 during those periods when A_1/A_o was large clearly establish that field-aligned streaming away from the near-equatorial current sheet is of fundamental importance in the mid-magnetosphere. In the outer magnetosphere the variation of θ_1 is much larger with

flow direction both toward and away from the equatorial plane. Again α_1 is generally between 140 to 180° and the flow is predominantly field-aligned.

In Fig. 13, the calculated values of the corotation anisotropy are compared with the values of $A_1/A_o \sin \theta_1$ for 0.5 - 2.15 MeV protons. $A_1/A_o \sin \theta_1$ represents the expected corotation anisotropy if gradient and field aligned flow effects are small. The predicted anisotropy is based on the energy spectra measured for a given hourly interval. This presentation provides a crude but effective overview of the expected effects of corotation. It is immediately apparent for the 0.5 - 2.15 MeV proton channel that the measured value of $A_1/A_o \sin \theta_1$ is almost always less than the expected value in the interval between 80 and 40 R_J.

This result suggests very strongly that complete corotation is not occurring in the outer magnetosphere. It is also obvious, however, that the dominance of field-aligned flow between 100 and 15 R_J introduces an added complexity. To separate these two effects, those 30 minute periods when the projection of the Jovian magnetic field in the plane of the spacecraft is within $\pm 20^\circ$ of the vertical direction have been selected. The field-aligned flow will then be contained between 340° and 20° or 160°-200° while the corotation anisotropy will be approximately orthogonal at 90°. Limiting the observation to those periods when the field projection is within $\pm$ 20° of normal to the ecliptic plane provides a means of separating the two effects.

It also greatly reduces the available data set and could introduce an observational bias by eliminating those periods when the planetary field has a large radial component.

In Fig. 14, the A_1/A_o and θ_1 values for those 30 min. periods which met the selection criteria samples are grouped in 6 polar plots by radial intervals. The position of the dots represent the magnitude and direction of the observed anisotropy. The three arrow heads in each plot are the computed minimum, average and maximum corotation anisotropies for the set of data points included in a given plot. The three intervals between 95 and 77 R_J demonstrate that the rest frame of the associated plasma is not rigidly rotating with the planet. There are 33 points in these plots and only 4 of them have a projection of ξ_{obs} onto the equatorial plane that is greater than 0.5 ξ_{cor}. These time periods for P-10-in are inside the magnetopause boundary and hence within the Jovian magnetosphere. The most straight-forward explanation is that radial outflow of the plasma must occur in this region. The data for the two intervals between 75 - 72.5 R_J and 66 - 53 R_J are not as clear and may represent partial corotation. Inside 45 R_J the observations are consistent with a rest frame which is rigidly rotating with the planet.

The next step in studying the anisotropies is to examine A_1/A_o, θ_1, and α_1 in a reference frame that is rotating with the planet - i.e. what is the variation of these quantities after the effects of corotation have been removed. The plots of A_1'/A_0', θ_1', and α_1', are shown in Fig. 15 for the 1.15 - 2.15 MeV energy interval between

50 and 15 R_J where corotation was observed to take place. The primed quantities indicate that the calculated corotation anisotropy has been approximately removed (small contributions from the A_2/A_o term were neglected). The product $A_1'/A_o' \sin \alpha_1'$ gives one component of the gradient anisotropy corresponding to a gradient which is perpendicular to the intersection of the scan plane with the plane perpendicular to $\bar{B}$. This component was generally less than 7% and no systematic gradient anisotropy at the level of 5% was present except possibly at three intervals near flux minima.

The quantity $A_1'/A_o' \cos \alpha_1'$ is the sum of two components; the projection of the field-aligned flow into the scan plane and the component of the anisotropy due to a gradient in the scan plane multiplied by sin θ_B (the angle between the magnetic field and the scan plane). Apparent field-aligned flow is the major contributor to our observations since the $A_1'/A_o' \sin \alpha_1'$ component appears to be negligible. Note that the peaks in A_1'/A_o' are even more sharply defined than those of A_1/A_o and correspond to large negative values of $A_1'/A_o' \cos \alpha_1'$. This indicates field-aligned flow towards the southern hemisphere of Jupiter when the spacecraft is south of the magnetic equator. At intensity maxima, when the spacecraft is just north of the magnetic dipole equator, A_1'/A_o' is reduced to the 3-5% range and $A_1'/A_o' \cos \alpha_1'$ is positive, corresponding to a field-aligned flow into the northern hemisphere. All three energy intervals show this behavior near the expected crossing of the equatorial current sheet. Although individual values are of limited significance, the consistent pattern when combined with the θ_1 and α_1 plots of figure 12, lend strong credence to the view that particles are being

injected from the current sheet and are flowing out towards the planetary polar region.

In the mid-magnetosphere the second harmonic A_2/A_o (Fig. 16) alternates between pancake ($\alpha_2 = 90^o$) and dumbbell ($\alpha_2 = 0^o$) distributions. Strong pancake distributions occur close to the equatorial current sheet (flux maxima). When corrected for magnetic field geometry, the dumbbell distributions appear to be strongest at the counting rate minima. These $\alpha_2 = 0^o$ values are characteristic of the large injection event at ∿1300 on 2 Dec. (Schardt et al., 1978).

The plot of J, A_1/A_o, θ_1 and α_1 for P-10-out is very different (Fig. 17). At the flux maxima A_1/A_o varies about a mean value of ∿20% and shows no trend with radial distance between 15 and 75 R_J. The angle θ_1 is close to 270^o from 15 - 90 R_J except for a few brief intervals near 45 R_J. In other words, this data set is consistent with the radial outward motion of energetic particles starting at 15 R_J. Just inside the magnetopause there are very large changes in A_1/A_o, θ_1, and α_1. For the flux maxima after December 4, 1973 the 2nd order anisotropy, A_2/A_o is perpendicular to B. This "pancake" distribution is similar to P-10-in and implies at least temporary trapping. Since injections at high field strength would produce a dumbbell distribution near the magnetic equator it is probable that a part of the injection region is at low field strength rather than near Jupiter.

The peak E (Fig. 17) at noon of December 6, 1973, was anomalous in that it consists of a succession of peaks which last for only 30 minutes each. Streaming both towards and away from Jupiter occurred. Streaming towards the planet tends to be associated with an appreciable

field aligned second order anisotropy. It would appear that field aligned acceleration of protons occurred further out at the magnetic equator and protons returning after mirroring together with incoming particles could be responsible for the dumbbell shape of the angular distribution. Simpson and McKibben (1976) made similar observations at the flux maximum at 200 on December 6, 1973, (peak D Fig. 17) which was not intense enough for detailed analysis with our instrument.

The intensity vs. time profiles of the P-11-in pass (Fig. 2, 18) suggest two different regions exist in the outer and mid-magnetosphere. Between 64 and 45 R_J no clearly defined 10 hr. periodicity exists and the flux levels are higher than those encountered between 45 and 15 R_J. During this latter period the magnetic field becomes almost radial. Under these conditions the corotation anisotropy and the field-aligned streaming are closely aligned in the scan plane of the detector system. The plots of intensity, θ_1, A_1/A_o and α_1 (Fig. 18) are different in several important aspects from those of P-10-in despite the close similarity of the two trajectories. While for P-11-in there are well-defined peaks in the A_1/A_o distribution, these peaks tend to be associated with flux maxima. A_1/A_o displays no well-defined radial dependence, and θ_1 shows a remarkably small variation about 90^o. Like P-10-in, the A_1/A_o peaks, inside 40 R_J have α_1 values close to 180^o. However, there are periods between 55 and 40 R_J when α is less than 40^o. These periods are clearly identified with reversals in the projection of the magnetic field into the scan plane and appear

to be associated with current-sheet crossings. Since changes in A_1/A_o and θ_1 at these crossings are very small, it may be concluded that the first order anisotropy is dominated by the corotation anisotropy.

Previously, the Iowa group (Van Allen, 1976) had shown that corotation of protons in the 0.6 - 3.4 MeV energy band was established just inside the magnetopause on this pass. The present analysis using the same methods described for P-10-in confirm their results.

Between 65 and 46 R_J, ~40% of the 30 minute periods were within $\pm 20^\circ$ of the vertical direction. The values of A_1/A_o and θ_1 for all of these periods are equal to or significantly larger than that expected for corotation (Fig. 19). This trend is established in less than 0.4 R_J of the last inbound magnetopause crossing. The larger than expected values of A_1/A_o are not understood at this time.

Inside 40 R_J, the magnetic field becomes essentially radial and α_1 is generally close to 180°. A_1/A_o is still appreciably larger than that expected for corotation but is now more consistent with a superposition of corotation and field-aligned flow.

The effect of transforming to a reference frame rotating with the planet (Fig. 20) is to generally reduce the magnitude of A_1'/A_o' by approximately a factor of 2. The value of $A_1'/A_o' \sin\theta_1'$ are often large especially just inside the magnetopause. $A_1'/A_o' \cos\theta_1'$ changes sign at the apparent current-sheet crossing providing further evidence that this region is the source of the observed particles.

The P-11-out trajectory was toward the noon meridian at mid-latitudes. The proton intensities during the early portion of this pass were

relatively low and highly variable. The first order anisotropies observed between 10 and 40 R_J were also small and variable (Fig. 21). Adjacent energy levels frequently did not give consistent values of θ_1 when averaged over the same 30 or 60 minute interval. Since the anisotropies are small during this period, they can be grossly distorted by counting rate variations. Near 40 R_J the particle intensity and the magnitude of A_1/A_o both increase. At the same time there are remarkable changes in θ_1 and α_1 apparently corresponding to several alternating periods of particle flow toward and away from the planet. However, when the effects of corotation are removed (Fig. 22), it is found that only the reversals just inside the magnetopause are significant.

There were a number of 30 minute time intervals between 27 and 56 R_J when the projection of the magnetic field in the scan plane was within $\pm 20^\circ$ of the vertical. Most of these periods resemble the P-10-in data between 75 and 53 R_J when the measured anisotropy frequently came from the expected direction but was less than half the magnitude predicted for corotation (Fig. 23).

When A_1/A_o, θ_1 and α_1 are corrected for corotation (Fig. 22), it is found that A_1'/A_o' is greatly reduced, but there are still many periods when the magnitude is in the range 20-40%. θ_1' is now centered about 270° and α_1' is generally $\leq 90^\circ$ with several periods approaching 0°. The reversal of θ_1 from 90 to 270° suggests that complete corotation may not be occurring at higher latitudes in the middle and outer magnetosphere but this situation is not as clear as P-10-in.

VI. DISCUSSION

The time histories, angular distributions and energy spectra of energetic protons have been systematically studied for the four passes of P-10 and 11 thru the outer and mid Jovian magnetosphere. Intercomparing the intensity time-histories from these passes indicate that both azimuthal and temporal changes are of great importance. There is generally a $\sim$15-20 R_J thick region just inside the magnetopause where the energy spectra are flatter, the intensity larger and the short-term temporal variations smaller than that encountered at slightly smaller radial distances. The energy spectra in the mid and outer regions are most frequently of the form $dJ/dP = C \exp -P/P_o$ [P = proton momentum]. P_o does not vary significantly until the inner-magnetosphere. On P-10-in there is a region inside the magnetopause where the corotation anisotropy is not observed. This result is interpreted in terms of a planetary wind although other explanations may be possible. Near the dawn meredian, particle streaming away from the planet is observed as close as 15 R_J. Inside 45 R_J corotation is clearly established. However, both the P-10-in and P-11-in mid-magnetosphere passes are dominated by apparent field-aligned streaming away from the current sheet region. The data strongly suggest that the proton component is not durably trapped.

A. Outer Magnetosphere

The proton anisotropies measured on P-10-in clearly established that corotation of energetic protons does not occur between $\sim$95 and $\sim$75 R_J. The anisotropies are either field aligned or randomly distributed and the component observed in the expected direction is much smaller than the

calculated values (Fig. 13, 14). The most straight forward interpretation is that of a reference frame moving radially - i.e. a "Jovian wind". The limits of our own heliosphere are defined by the thermally driven solar wind. Centrifugally-driven stellar winds have been studied as a means of efficiently removing angular momentum from stellar systems (Schatzmann, 1962; Mestel, 1968). The possible existence of a planetary wind in the outer Jovian magnetosphere has been postulated prior to the P-10 and 11 encounters (Ioannidis and Brice 1971, Michel and Sturrock 1974). Radial outflow was expected to begin when the centrifugal force on the plasma exceeds the magnetic field stress. A simple approximate expression for this distance is given by the Alfven radius where the magnetic energy density equals the corotation energy density of the plasma (Hill et al. 1974, Kennel and Coroniti, 1977) i.e.

$$B^2/8\pi = 1/2\ \rho\ \Omega^2\ R_A^2$$

This relation is equivalent to defining the Alfven radius, R_A as the point where the corotation velocity is equal to the Alfven speed. The key unknown is the plasma density ρ. For P-10-in partial corotation appears at $\sim$75 R_J. This value can be used to calculate a lower limit to the plasma density at this point of $N_A \sim 10^{-2}$ ions/cm^3 for $\mu = 1$.

The polar wind will be terminated at a radial distance $R_\beta = L_\beta R_J$ where the pressure of the wind is balanced by that of the solar wind, i.e.

$$\rho_{s.w.} U^2_{s.w.} = \rho \Omega L_A^2 R_J^2 \times (L_A/L_\beta)^2$$

The classical magnetopause distance, D, is on the order of 41 R_J and varies as $U^{1/3}_{s.w.}$ and $P^{1/6}_{s.w.}$. As Kennel and Coroniti (1977) have emphasized for $R_A \geq D$, a super-Alfvenic planetary wind should develop.

This interpretation is consistent with the magnetic field model of Goertz et al. (1976) who find the last closed field line at 70 R_J for P-10-out. Open field lines at higher latitude should then be found considerably closer to Jupiter, and the lack of corotation at $\sim 45^o$ latitude is evident in the P-11-out pass (Fig. 23). The complex topology of Jupiter, however, may allow other explanations. Goertz (1978a) has cautioned that this simple approach for defining the planetary wind region neglects magnetic stresses and that the off-diagonal terms of the stress-tensor are especially important in the region close to the Jovian current-sheet. Siscoe (1978) has concluded that the plasma density may be lower than that required for a super-Alfvenic wind. In fact, the data on both P-10-in and P-11-out suggest there are intermediate regions where only partial corotation occurs. Sentman and Van Allen (1976) reported bi-directional streaming of electrons in the outer magnetosphere (P-10-in). This is suggestive of durable or quasi-trapping, but as they already pointed out open field lines having kinks and many backscattering centers can also produce such angular distributions. Similar bi-directional

streaming of electrons was observed both in this region and in the magnetosheath (Goddard-New Hampshire experiment) thus confirming that these distributions do not provide evidence as to whether or not the magnetic field lines are open or closed.

In the dawn hemisphere the outward streaming of plasma may start considerably closer to Jupiter than 70 R_J. Kivelson et al. (1978) found that the sweep back of the magnetic field lines can be interpreted in terms of a planetary wind starting at 33 to 43 R_i with a velocity of 600 to 840 km/sec. If the energetic particles observed on P-10-out reflect the velocity of the thermal plasma, then the radial component of A_1/A_o (Fig. 17) can be interpreted in terms of the plasma velocity. The average velocity increased from 160 km/sec at 15 R_J to 330 km/sec at 50 R_J with a substantial scatter between different observations, extreme values being 130 km/sec observed at 17.4 R_J and 360 km/sec at 50.5 R_J. Since a consistent southward magnetic field is found inside the current sheet, the frozen-in field-line picture discussed above requires lack of azimuthal symmetry around Jupiter for distances < 70 R_J. Goertz (1978a) offered an alternate explanation based on cross-field diffusion of the plasma inside the current sheet and pointed out that the required diffusion coefficient is much smaller than the Bohm diffusion coefficient.

B. The Middle-Magnetosphere

The angular distribution of energetic ions between 50 and 20 R_J show a very strong azimuthal variation. The large amplitude of these anisotropies was noted in the original study of P-10-in by Trainor et al. (1974) and subsequent work (McDonald and Trainor 1976) established that it

was due to field-aligned streaming. Near the dawn meridian outward streaming along the almost radial field lines is observed. At $\sim 40^{\circ}$ from the earth-sun line, field-aligned streaming toward the planet is the dominant feature when the spacecraft is located away from the equatorial current sheet. At mid-latitudes near the sub-solar region, the anisotropies are smaller and there are periods of flow both toward and away from the current sheet.

The streaming anisotropy is on the order of 18% for P-10-in. This magnitude is not strongly dependent on energy or radial distance between 45 R_J and 20 R_J. Such an anisotropy must be produced either by changes in the particle energy or by physically removing them. If the changes take place in energy space, then an energy loss of $\sim$200 keV/particle in a half bounce period is required for the 1.1-2.15 MeV proton observations. Physically removing the particle means that $\sim$20% of the particles moving down the field line do not return. The time scale for these processes is formidable $\approx$600 sec. at 40 R_J. Associated with the A_1/A_o peaks is a significant 2nd order component, A_2/A_o with θ_2 being closely aligned with the magnetic field.

There are a number of physical processes which could play a role in producing the observed anisotropies. These include:

a. Spatial intensity gradients in the particle distribution function.

b. Energy loss by coulomb collisions

c. Particle loss by charge exchange

d. Parallel electric fields

e. Perpendicular electric fields

f. Preferential scattering by electromagnetic waves travelling along field lines

g. Diffusion processes.

h. Azimuthal asymmetry in particle population.

(a) Gradients: Northrop et al. (1979) have shown that the observed value of A_1/A_o appears to be too large to be produced by realistic intensity gradients in the particle distribution. It is important that this analysis be extended to lower energies. The very small values of $A_1'/A_o \sin \theta_1'$ (Fig. 15) provide further evidence that the effects of gradient anisotropies are generally very small.

(b, c) Energy or Particle Loss: To produce the observed anisotropies by coulomb collisions requires a mean energy loss/particle/half hour period of $\sim$200 keV. The 1 MeV protons must traverse a region with an average density $>10^8$ atoms/cm^3 to produce this energy loss. Such a value implies that particles mirror at altitudes lower than 600 km. Similar densities are required for charge exchange processes at 1 MeV.

(d) Parallel Electric Fields: Electric fields parallel to B are known to produce field-aligned streaming of both electrons and ions in the earth's auroral zone. The Jovian particle distributions do not appear to be consistent with such a field. The proton energy spectra become softer with increasing distance from the equator which is the opposite of what would be expected for particles which have been accelerated through a potential. Also there is no streaming of the electrons in the opposite direction. The electron anisotropy is small and highly variable.

When examined over 15 minute intervals between 46 and 17 R_J, only 8% of the electron angular distributions had consistent values of A_1/A_o above 4%. Of these 16 intervals only 2 were streaming in a direction opposite to the protons.

(e) Perpendicular Electric Fields: An electric field normal to $\vec{B}$ produces a convection velocity

$$\vec{V}_C = \frac{\vec{E} \times \vec{B}}{B^2}$$

The polarization field across the magnetosphere produced by the solar wind will give rise to cross field motion in those regions which are not shielded from it.

Outward convection produces a net reduction in the particle flux by volume expansion and by energy loss if the first invariant is conserved. In that case $\Delta R/R \approx A_1'/(1+2\gamma)A_o'$, where γ is the index of a power law approximation to the energy spectrum. In this expression it is assumed that the equatorial flux is independent of R (20 to 45 R_J) and that particles returning after mirroring actually originated at an equatorial distance ΔR closer to the planet. At 40 R_J, the distance ΔR is about 1.5 R_J for 0.6 MeV protons and has to be covered in one half bounce period, thus requiring a convection velocity of $\sim$200 km/sec. The protons do not actually drift this distance at the equator but all along the flux tube; however, the net time required is the same if the field lines are equipotentials. A dusk to dawn field across the magnetosphere of 2×10^{-3} v/meter would produce the required convection velocity provided the inner region is not shielded from it.

The electric polarization field induced by the solar wind is $\bar{E} = -\bar{V}_{sw} \times \bar{B}_{sw}$ and from this we obtain the convection velocity to be approximately $V_C \simeq -V_{sw} B_{sw}/B$. For P-10-in during the time of interest, a fast solar wind stream was passing over Jupiter, thus $V_{sw} \simeq 600$ km/sec and $B_{sw} \simeq 3\gamma$ giving the required convection velocity of 200 km/sec in the 10 γ field at 40 R_J. Since the expected range in convection electric fields is $0.3 - 2.2 \times 10^{-3}$ volts/m, corresponding to 30-220 km/sec, one would expect to observe quite different anisotropies at different times (Smith et al. 1978). This process can also explain the tendency for dumbbell distributions away from the equator, because the conservation of the first invariant will decrease $E_\perp$ proportionally to the decrease in B while leaving $E_{\parallel}$ unchanged.

(f) Acceleration by EM Waves: Barnes (1968) has shown that electromagnetic waves travelling along field lines can preferentially increase the proton velocity along the field line and hence could partially produce the observed streaming. Furthermore those waves which move along the field will preferentially heat ions and will be less effective for electrons. Again the softer energy spectra at the time of A_1/A_o maxima does not appear to support this type of process.

(g) Diffusion: Beyond 20 R_J the observed magnetic field differs significantly from the planetary dipole field and the perturbation field dominates beyond 35 R_J. This field is due to magnetospheric currents and fluctuates considerably about its mean value (Smith et al. 1976; Kivelson et al. 1976). If scattering by these field irregularities should

dominate particle trajectories, then the adiabatic invariants would not be conserved and diffusion theory becomes applicable. The following approximate equations (Jokipii and Parker 1970) apply in the corotating frame of reference if the particle energy is not changed in the scattering process:

$$\xi_{\parallel}(E) = \frac{-3K_{\parallel}}{V}\frac{\partial \ln U(E)}{\partial s}$$

$$\xi_{\perp}(E) = \frac{-3K_{\perp}}{V}\frac{\partial \ln U(E)}{\partial x}$$

$$\lambda = \frac{3K_{\parallel}}{V}$$

$$\frac{K_{\perp}}{K_{\parallel}} \simeq \frac{R_g^2}{R_g^2 + \lambda^2}$$

where $U(E) = \frac{4\pi J(E)}{V}$ is the particle density, $\xi_{\parallel}$ and $\xi_{\perp}$ are anisotropies measured parallel and perpendicular to the magnetic field, with s the coordinate parallel to $\vec{B}$ and x the coordinate perpendicular to $\vec{B}$ in the direction in which $\xi_{\perp}$ was observed. $K_{\parallel}$ and $K_{\perp}$ are the two major components of the diffusion tensor, λ the mean free path, R_g the gyroradius.

A detailed analysis of P-10-in mid-magnetospheric data by Schardt and Birmingham (1979) established that indeed the proton intensity along a given field line decreases more rapidly than would be expected by the straight forward application of adiabatic theory and Liouville's theorem. They find that the 0.6 MeV proton flux decreases by a factor

of 3 in 12 R_J giving a gradient (or a logarithmic derivative) of 1.3×10^{-11} per cm. This figure combined with the field-aligned anisotropy of 18% gives the following values:

$$K_{\parallel} = 5 \times 10^{18} \text{ cm}^2 \text{ sec}^{-1}$$

$$\lambda = 1.4 \times 10^{10} \text{ cm} = 2 R_J$$

where λ can be regarded crudely as the distance over which a particle will be scattered through $\sim 90^{\circ}$.

It is important to estimate the time required for this process to reach equilibrium. If it is assumed that particles are injected at t = 0 and S = 0 in an infinite medium with a diffusion coefficient κ, then at a distance = S, maximum intensity will be reached at $t = t_{MAX}$ where

$$t_{MAX} = \frac{S^2}{6\kappa} \simeq 100 \text{ sec at } 8 R_J \text{ inside the medium.}$$

At this time the streaming anisotropy will approach 0 and the system is near equilibrium. Since this time is small compared to the bounce period, the magnetosphere must be near equilibrium, and the anisotropy and intensity gradient can be maintained only by a source near the equator and sink along the field lines.

A value for the diffusion coefficient perpendicular to the magnetic field can be derived from $\kappa_{\parallel}$, λ, and Rg:

$$\kappa_{\perp} \simeq 2 \times 10^{17} \text{ cm}^2 \text{ sec}^{-1}$$

This coefficient can also be estimated from the observed anisotropy perpendicular to the magnetic field, and the perpendicular flux gradient. As can be seen from figure 11 CD, near flux minimum the projection of the

field points approximately towards 240°, and $\xi_\perp = A_1'/A_0' \sin \alpha_1' \simeq +3$ to 5% (Fig. 15). Only one value of 20% exceeds this figure significantly. The direction of $\xi_\perp$ is consistent with increasing flux towards the equator. At a radial distance of 30 R_J on either side of flux minimum, the magnetic equator moves south about 3 R_J per hr while the flux doubles. The gradient of 3.2×10^{-11} per cm gives $\kappa_\perp \simeq 5 \times 10^{17}$ $cm^2 sec^{-1}$. Considering the uncertainties involved, the two values for $\kappa_\perp$ are in reasonable agreement.

Beyond 40 R_J, $\kappa_\perp$ would be expected to approach $\kappa_\parallel$ because the gyroradius could become large compared to the mean free path, $\kappa_\perp \simeq \kappa_\parallel Rg^2/(Rg^2+\lambda^2)$. Although we do not know how λ changes with distance, we know that $Rg^2 \propto B^{-2} \propto R^4$. Therefore, cross-field diffusion of protons may be very rapid in the outer magnetosphere.

The P-11-in and out passes agree qualitatively with the diffusion picture. During P-11-out there were periods when the field-aligned flow was away from Jupiter and $\alpha' > 90°$ (Figure 22). During these periods Pioneer was apparently on field lines that were partially open with a sufficiently small λ that the observed particle population can be derived from cross-field diffusion which occurred between the spacecraft and Jupiter. The P-10-out pass, however, is inconsistent with this picture. In the region between 30 and 60 R_J, the flux boundaries are exceedingly sharp with the flux increasing by a factor of 1000 in 100 seconds. If we assume that the boundary moved across the spacecraft at the local Alfvene speed, $\sim 10^3$ km/sec, this large a gradient must be maintained over a distance of less than 1.5 R_J. The particle behavior

on this pass is best understood from the work of Goertz (1976) who finds that both the magnetic field and particle data are consistent with open field lines occurring a few R_J away from the current-sheet region, but even in this model substantial cross field diffusion may occur in the current sheet.

Nishida (1976) proposed a diffusion model in which the first adiabatic invariant is conserved, $\lambda >> 2\ R_J$. Qualitatively, this model predicts streaming in the mid-magnetosphere - towards the planet at low latitude and away at higher latitude - just as observed. The processes proposed by Nishida may definitely contribute to our observations (Sentman et al. 1978), but they cannot explain the field-aligned flux gradient (Schardt and Birmingham 1979). Since the first invariant is conserved, the process is also not consistent with lack of a definite radial dependence of the proton energy spectra.

(h) Azimuthal Asymmetry: Goertz (1978b) has proposed an acceleration process based on the adiabatic increase in energy as the drift path takes particles from a low field strength at midnight into a much stronger field at noon. This model requires trapping over a drift orbit and thus represents a completely different approach from (g). If we use the two proposed field models for the dawn and noon sectors (Goertz et al. 1976; Barrish and Smith 1975) then the field strength increases in 2.5 hrs by an order of magnitude along the drift path of an equatorially mirroring particle. Consequently such a particle would gain a factor of 10 in energy while small pitch angle particles would be relatively unaffected.

We can describe what happens qualitatively by following only equatorial particles and by using the average rate at which the field increases along the drift path. In the absence of scattering, a strong azimuthal flux gradient would exist with respect to the subsolar point. A fixed System III longitude would rotate through it, and protons returning to the equator after mirroring would have left the equator 1/2 bounce period towards dawn. If we compare equatorial energies and fluxes at a given energy separated by 500 seconds, ∿1/2 bounce period, we find

$$\frac{E_2}{E_1} = \frac{B_2}{B_1} = 1.05$$

$J_2/J_1 = 1.17$ for 0.6 MeV protons.

If we now introduce enough scattering that particles about 8 R_J below the equator still reflect the equatorial distribution, then at P-10-in flux minima, protons with 0-90° pitch angles would just have left the equator while protons with 90-180° pitch angles left the equator ∿500 seconds earlier. The ratio of flux parallel and anti-parallel to $\overline{B}$ would then reflect the equatorial azimuthal flux gradient. The azimuthal gradient would be reduced by the proposed scattering process. Qualitatively, therefore, this process could also account for the P-10-in angular distributions and for the large flux ratio between P-10-in and P-10-out.

In summary it appears that among the known processes: perpendicular electric fields, diffusion processes or azimuthal asymmetries in the particle population could explain the field-aligned proton streaming; however, the presently available data cannot establish which one or if any are actually playing a major role. Both the transverse electric field

and particle diffusion processes remove energetic particles rapidly from the trapping region and require an equatorial particle source. The energy required to maintain the particle streaming can be estimated on the basis of a loss into the southern hemisphere of $\sim 5 \times 10^{3}$ protons/cm^2-sec with an average energy of 0.65 MeV. This loss of 5×10^{-3} ergs/cm^2-sec could be 2.6 times as much, based on extrapolation to lower energies using an exponential momentum spectrum. If this energy is supplied over one quandrant into both hemispheres between 20 and 40 R_J, then we would need $E_{total} \approx 10^{21}$ ergs/sec. In contrast, explanation (h) based on a strong azimuthal asymmetry in energy would require a much smaller energy source. In the model proposed by Goertz (1978b) trapping lifetimes are at least of the order of a planetary rotation period, 10 hrs, and most of the energy gained in the dawn sector is pumped back into the magnetosphere in the dusk sector.

This discussion centered on explaining observations from the P-10-in pass. Differences between it and the P-10-out pass were attributed to azimuthal asymmetry relative to the Jupiter-Sun line, and differences with P-10-out were explained in terms of the higher latitude covered. P-10-in and P-11-in covered, however, almost the same region of space (Figure 1), yet differed substantially in many respects (figures 2, 12, 18). These differences can be explained in terms of changes in solar wind conditions. As Smith et al. (1978) have shown, a fast solar stream coincided with Pioneer 10's passage through the mid-magnetosphere. This order of magnitude increase in dynamic pressure resulted in a thicker and

hotter equatorial plasma sheet and probably also an increased flux of energetic protons. In contrast, Pioneer 11 passed through the mid-magnetosphere when the pressure of the solar wind dropped from a slight enhancement to a minimum value. In the thinner and colder equatorial plasma sheet, the centrifugal force played a greater role than in the case of Pioneer 10. Thus the plasma equator did not dip down as far as the "dipole equator" and Pioneer 11 never entered the plasma sheet after it passed 40 R_J. This conclusion is based on the characteristics of the magnetometer records of Kivelson et al. (1977). A contributing factor to a thinner plasma sheet was that the P-11-in trajectory was closer to dawn (Figure 1).

Much more data are needed before we can identify the processes that shape the Jovian Magnetosphere. The Voyager I and II studies will be carried out closer to the current-sheet region so it will not be possible to duplicate many of the observations reported here. However, studies of lower energy particles and extended measurements of waves and plasma and the first transversal of the tail region should provide increased understanding of the very complex and dynamic Jovian magnetosphere.

Acknowledgements

The authors are indebted to Dr. E. Smith for 1 minute and 1 hour averaged magnetic field data. Discussions with Drs. C. K. Goertz and T. G. Northrop are greatfully acknowledged.

TABLE I

LET II PARAMETERS

a. RATES

COINCIDENCE CONDITION	PROTON ENERGY (MeV)	ALPHA ENERGY (MeV/nucleon)	COMMENTS
$SI_1 \overline{SII}\ \overline{SII_A}\ \overline{SIII}$	0.20 - 2.15	0.07 - 2.05	For P-10:24 sec. count 96 sec. repeat
$SI_2 \overline{A}_1$*	0.76 - 2.15	0.22 - 2.05	For P-11:12 sec. count 48 sec. repeat
$SI_3 \overline{A}_1$	1.25 - 2.15	0.34 - 2.05	
$SI_4 \overline{A}_1$		0.66 - 2.05	
$SI_6 \overline{A}_1$	0.52 - 2.15	0.16 - 2.05	Sectored Rates 1.5 sec per 45°
$SI_7 \overline{A}_1$	1.15 - 2.15	0.32 - 2.05	Repetition:
$SI_8 \overline{A}_1$	P-10 1.79 - 2.15 P-11 1.47 - 2.15	0.48 - 2.05 0.40 - 2.05	P-10 192 sec. P-11 140 sec.

b. DIFFERENTIAL ANALYSIS

$SI_1 \overline{A}_1 - SI_6 \overline{A}_1$	0.20 - 0.52	0.07 - 0.16	Sectored rates were spin averaged
$SI_6 \overline{A}_1 - SI_2 \overline{A}_1$	0.52 - 0.76	0.16 - 0.22	
$SI_2 \overline{A}_1 - SI_3 \overline{A}_1$	0.76 - 1.25	0.22 - 0.34	
$SI_3 \overline{A}_1 - SI_4 \overline{A}_1$	1.25 - 2.15	0.34 - 0.66	
$SI\ SII_1 \overline{A}_2 - SI\ SII_2 \overline{A}_2$**	3.2 - 5.7	above 2.2	
$SI\ SII_2 \overline{A}_2 - SI\ SII_3 \overline{A}_2$	5.7 - 14.8	above 2.5	

*$\overline{A}_1 \equiv \overline{SII}\ \overline{SII_A}\ \overline{SIII}$

**$\overline{A}_2 \equiv \overline{SII_A}\ \overline{SIII}$

Geometric Factor: 0.0155 cm^2-ster.

TABLE II

LET I PARAMETERS

a. RATES

COUNTER THRESHOLD	PROTON ENERGY (MeV)	ALPHA ENERGY (MeV/NUCLEON)	COMMENTS
DI_2	0.60	0.39	DI_2 also sensitive to electrons
DI_4	0.84	0.46	P-10:24 sec. count 192 sec. repetition
DI_5	1.12	0.53	P-11:12 sec. count 96 sec. repetition
DI_6	1.60	0.63	
DI_7	2.29	0.77	

b. DIFFERENTIAL ANALYSIS

$DI_2 - DI_4$	0.60-0.84	0.39-0.46
$DI_4 - DI_5$	0.84-1.12	0.46-0.53
$DI_5 - DI_6$	1.12-1.60	0.53-0.63
$DI_6 - DI_7$	1.60-2.29	0.63-0.77

ΔE vs. E analysis:

Protons above 3.4 MeV 1 MeV channels

Alphas above 0.9 MeV/n 0.25 MeV/n channels

Geometric Factor: 1.56 cm^2-ster. for integral thresholds

0.15 cm^2-ster. for ΔE vs. E

REFERENCES

Barish, F. D., and R. A. Smith, An analytical model of the Jovian magnetosphere, Geophys. Res. Lett., 2, 269, 1975.

Barnes, A., Collisionless heating of the solar-wind plasma I. Theory of the heating of collisionless plasma by hydromagnetic waves, Astrophys. J., 154, 751, 1968.

Dessler, A. J. and T. W. Hill, Jovian Longitudinal control of Io-related radio emissions, submitted to Ap. J., 1978.

Fillius, R. W., The trapped radiation belts of Jupiter, in Jupiter, T. Gehrels, ed., Univ. of Arizona Press, p. 896, 1976.

Goertz, C. K., The Jovian magnetodisk, U. Iowa Report 78-27, 1978a.

Goertz, C. K., Energization of charged particles in Jupiter's outer magnetosphere, J. Geophys. Res., 83, 3145, 1978b.

Goertz, C. K., D. E. Jones, B. A. Randall, E. J. Smith, and M. F. Thomsen, Evidence for open field lines in Jupiter's magnetosphere, J. Geophys. Res., 81, 3393, 1976.

Hill, T. W., A. J. Dessler, and F. C. Michel, Configuration of the Jovian magnetosphere, Geophys. Res. Lett., 1:3-6, 1974.

Intriligator, D. S., and J. H. Wolfe, Results of the plasma analyzer experiment on Pioneers 10 and 11, in Jupiter, ed. T. Gehrels, Univ. of Arizona Press, 848, 1976.

Ioannidis, G., and N. M. Brice, Plasma densities in the Jovian magnetosphere:Plasma slingshot or Maxwell demon? Icarus, 14:360-373, 1971.

Jokipii, J. R., and E. N. Parker, On the convection, diffusion and adiabatic deceleration of cosmic rays in the solar wind, Astrophys. J., 160, 735, 1970.

Kennel, C. F. and F. V. Coroniti, Jupiter's magnetosphere, Annual Review of Astronomy and Astrophysics, 15, 389, 1977.

Kivelson, M. G., P. J. Coleman, Jr., L. Froidevaux, and R. L. Rosenberg, A time dependent model of the Jovian current sheet, J. Geophys. Res., 83, 4823, 1978.

Kivelson, M. G., P. J. Coleman, Jr., R. L. Rosenberg, and E. J. Smith, Jupiter's magnetospheric field from measurements of the helium vector magnetometers on pioneers 10 and 11 - A compendium of plots, UCLA Publication Number 1702, 1977.

Kivelson, M. G., Jupiter's distant environment, UCLA, Inst. Geophys. and Planet. Phys. publication 1582, 1976.

McDonald, F. B., and J. H. Trainor, Observations of energetic Jovian electrons and protons, in Jupiter, T. Gehrels ed., Univ. of Arizona Press, p.961, 1976.

Mestel, L., Magnetic breaking by a stellar wind, 1, Mon. Notic. Roy. Astron. Soc., 138, 359, 1968.

Michel, F. L., and P. A. Sturrock, Centrifugal instability of the Jovian magnetosphere and its interaction with the solar wind, Planet. Space Sci., 22:1501-1510, 1974.

Nishida, A., Outward diffusion of energetic particles from the Jovian radiation belt, J. Geophys. Res., 81, 1771, 1976.

Northrop, T. G., T. J. Birmingham, and A. W. Schardt, Anisotropies in the flux of Pioneer 10 protons, J. Geophys. Res., (submitted for publication) 1979.

Schardt, A. W., and T. J. Birmingham, Discrepancy in proton flux extrapolation along field lines in the middle Jovian magnetosphere, to be published in J. Geophys. Res., 1979.

Schardt, A. W., F. B. McDonald, and J. H. Trainor, Acceleration of protons at 32 Jovian radii in the outer magnetosphere of Jupiter, J. Geophys. Res., 83, 1104, 1978.

Schatzman, E., Loss of angular momentum by stellar wind, Ann. Astrophys., 25, 1, 1962.

Sentman, D. D., J. A. Van Allen, and C. K. Goertz, Correction to "Recirculation of Energetic Particles in Jupiter's Magnetosphere", Geophys. Res. Letters 5, 621, 1978.

Sentman, D. D. and J. A. Van Allen, Angular distributions of electrons of energy E_e > 0.06 MeV in the Jovian magnetosphere, J. Geophys. Res., 81, 1350, 1976.

Simpson, J. A., and R. B. McKibben, Dynamics of the Jovian magnetosphere and energetic particle radiation, in Jupiter, T. Gehrels ed., Univ. of Arizona Press, p.738, 1976.

Siscoe, G. L., Jovian plasmaspheres, J. Geophys. Res., 83, 2118, 1978.

Smith, E. J., R. W. Fillius and J. H.Wolfe, Compression of Jupiter's magnetosphere by the solar wind, J. Geophys. Res., 83, 4733, 1978.

Smith, E. J., L. Davis, Jr., and D. E. Jones, Jupiter's magnetic field and magnetosphere, in Jupiter, T. Gehrels, ed., Univ. of Arizona Press, p.788, 1976.

Trainor, J. H., F. B. Mcdonald, B. J. Teegarden, W. R. Webber, and E. C. Roelof, Energetic particles in the Jovian magnetosphere, J. Geophys. Res., 79, 3600-3614, 1974.

Van Allen, J. A., High energy particles in the Jovian magnetosphere, in Jupiter, T. Gehrels, ed., Univ. of Arizona Press, p. 928, 1976.

Zwickl, R. D., and W. R. Webber, Limitations of the COS approximation as applied to the cosmic-ray anisotropy, Nuc. Instr. and Methods, 138, 191-199, 1976.

FIGURE CAPTIONS

Figure 1 Meridonal and equatorial projections of the Pioneer 10 and 11 encounter trajectories. The various orientations of the scan plane are indicated. Note that the Pioneer spin axis was in the plane of the ecliptic.

Figure 2 Proton fluxes observed during the inbound pass of Pioneer 10 and 11. The energy ranges shown are 0.2 - 0.5 MeV and 1.1 - 1.6 MeV. The bow shock and magnetopause crossings are indicated by the arrows labeled M and S with those of P-11 enclosed in a circle. Both data sets have been plotted on similar time scales which have then been aligned at 60 R_J. The tick marks along the abscissa represent 24 hour intervals. The radial position of each spacecraft is indicated along the top of the figure.

Figure 3 Flux of 0.2 to 0.5 MeV protons observed during the outbound pass of Pioneer 10. Superimposed is the Pioneer 11 inbound flux. Alignment of the time (and radial distance) scale was done so that the first two peaks were superimposed.

Figure 4 Comparison of proton fluxes (0.2 to 0.5 and 1.1 to 1.6 MeV) observed during the Pioneer 10-in and Pioneer 11-out passes. The format is the same as that described in figure caption 2 except the distance scales are aligned at 45 R_J.

Figure 5 Proton energy spectra for representative hourly intervals in the outer magnetosphere near 40° towards dawn from

the subsolar direction as observed by Pioneer 10. In the outer magnetosphere there is generally good agreement with a simple power-law in kinetic energy. In the mid-magnetosphere the spectra can no longer be described by a single power law. The X's represent LET II differential flux values, and the O's are differential single parameter values from LET I. The P's are fluxes obtained by multi-parameter analysis using the LET pulse height data.

Figure 6 Proton momentum spectra for hourly intervals in the middle magnetosphere near 25^{o} from the subsolar direction as observed by Pioneer 10. The data are well represented by the spectral form exp $(-P/P_{o})$. The symbols are the same as those used in Fig. 5. Due to counter saturation, LET I data could not be used at 13.1 and 12.1 R_{J}.

Figure 7 Spectral indicies for proton spectra (averaged over hourly intervals) observed during Pioneer 10-in. γ is the exponent in a power law spectrum in energy $\propto E^{-\gamma}$, and P_{o} is the e-folding momentum for an exponential momentum spectrum of the form exp $-P/P_{o}$. The top set of arrows labeled S and M are the shock and magnetopause crossings. The lower, unlabeled set of arrows represent well defined intensity maxima (Fig. 2).

Figure 8 Spectral indicies P_{o}, for proton spectra observed during the Pioneer 10 out-bound pass. Arrows represent the center of the intensity maxima.

Figure 9 Spectral indicies, P_o, for proton spectra observed during the Pioneer 11 passes. The format is similar to that of Fig. 7.

Figure 10 Geometry of angular distribution data. The direction of the first order anisotropy is specified by θ_1 relative to North ecliptic, and by α_1 relative to the projection of the magnetic field into the scan plane. Note θ_1 is measured counter clockwise. θ_1 represents the direction from which the protons appear to come; $\theta_1 + \pi$ is the direction toward which they are moving.

Figure 11 Characteristic angular distributions in the subsolar hemisphere. Distributions A, B, C, and D were observed at the corresponding flux maxima shown in figure 12 and distributions AB, BC, CD at the respective intensity minima.

Figure 12 Fluxes and first order anisotropies of 0.5 - 2.15 (dashed) and 1.15 - 2.15 MeV protons from P-10-in. θ_1 is the direction from which A_1/A_o is seen, and α_1 is the angle between θ_1 and the projection of the magnetic field in the scan plane.

Figure 13 Comparison of first order anisotropy due to rigid corotation (histogram) with observed anisotropies (points) in the

corotation direction for 0.5 - 2.15 MeV protons (P-10-in). The dashed lines are drawn at the time of intensity maxima (Fig. 12).

Figure 14 Measured Pioneer 10 anisotropies A_1/A_o in the scan plane and the anticipated corotation anisotropy during those periods when the projection of B in the scan plane was within $\pm 20^o$ of the vertical direction. The three arrow heads indicate the minimum, average and maximum, respectively of the expected corotation anisotropy based on the measured energy spectra.

Figure 15 First order anisotropies corrected for Jupiter's rotation. A_1'/A_o', θ_1', and α_1' of 1.15 - 2.15 MeV protons as they would be observed in a corotating coordinate system for the P-10-in pass. θ_1' is the direction from which A_1'/A_o' is seen, and α_1' is the angle between θ_1' and the projection of the magnetic field into the scan plane (Fig. 10). Dashed lines indicate flux maxima A B C D as shown in Figure 12. $A_1'/A_o' \sin \alpha_1'$ is one component of the anisotropy perpendicular to $\overline{B}$, and $A_1'/A_o' \cos \alpha_1'$ is primarily due to the projection into the scan plane of the field-aligned streaming.

Figure 16 Pioneer 10 inbound, second order anisotropy, A_2/A_o, and the angle between the projection of the magnetic field and the axis through the maxima in the bidirectional part of the angular distribution. No corrections have been made for counter geometry or for the magnetic field direction relative to the scan plane.

Figure 17 Proton fluxes and first order anisotropy A_1/A_o, θ_1 and α_1 observed during the outbound pass of Pioneer 10 for 0.5 - 2.15 MeV (dashed) and 1.15 - 2.15 MeV protons.

Figure 18 Fluxes and first order anisotropy A_1/A_o, θ_1 and α_1 of 0.5 - 2.15 MeV (dashed) and 1.15 - 2.15 MeV protons for the inbound pass of Pioneer 11.

Figure 19 Pioneer 11 inbound observations of the first order anisotropy component in the corotation direction (solid histogram) along with the expected anisotropy from rigid corotation (dashed histogram) for 0.54 - 2.15 MeV protons. The dots designate periods when the field was within 20^o of vertical.

Figure 20 First order anisotropy of 0.54 - 2.15 MeV protons corrected for Jupiter's rotation observed during the P-11-in pass (same notation as Fig. 15).

Figure 21 Fluxes and first order anisotropy A_1/A_o of 0.54 - 2.2 MeV (dashed) and 1.15 to 2.15 MeV protons observed during the outbound pass of Pioneer 11 at moderately high magnetic latitudes.

Figure 22 Pioneer 11 outbound pass, first order anisotropy of 0.54 - 2.15 MeV protons corrected for Jupiter's rotation (same notation as Fig. 15).

Figure 23 Corotation anisotropy (dashed histogram) and Pioneer 11 outbound observations of first order anisotropy component in corotation direction (solid histogram) for 0.54 to 2.15 MeV protons. The dots designate periods when the field was within 20° of vertical.

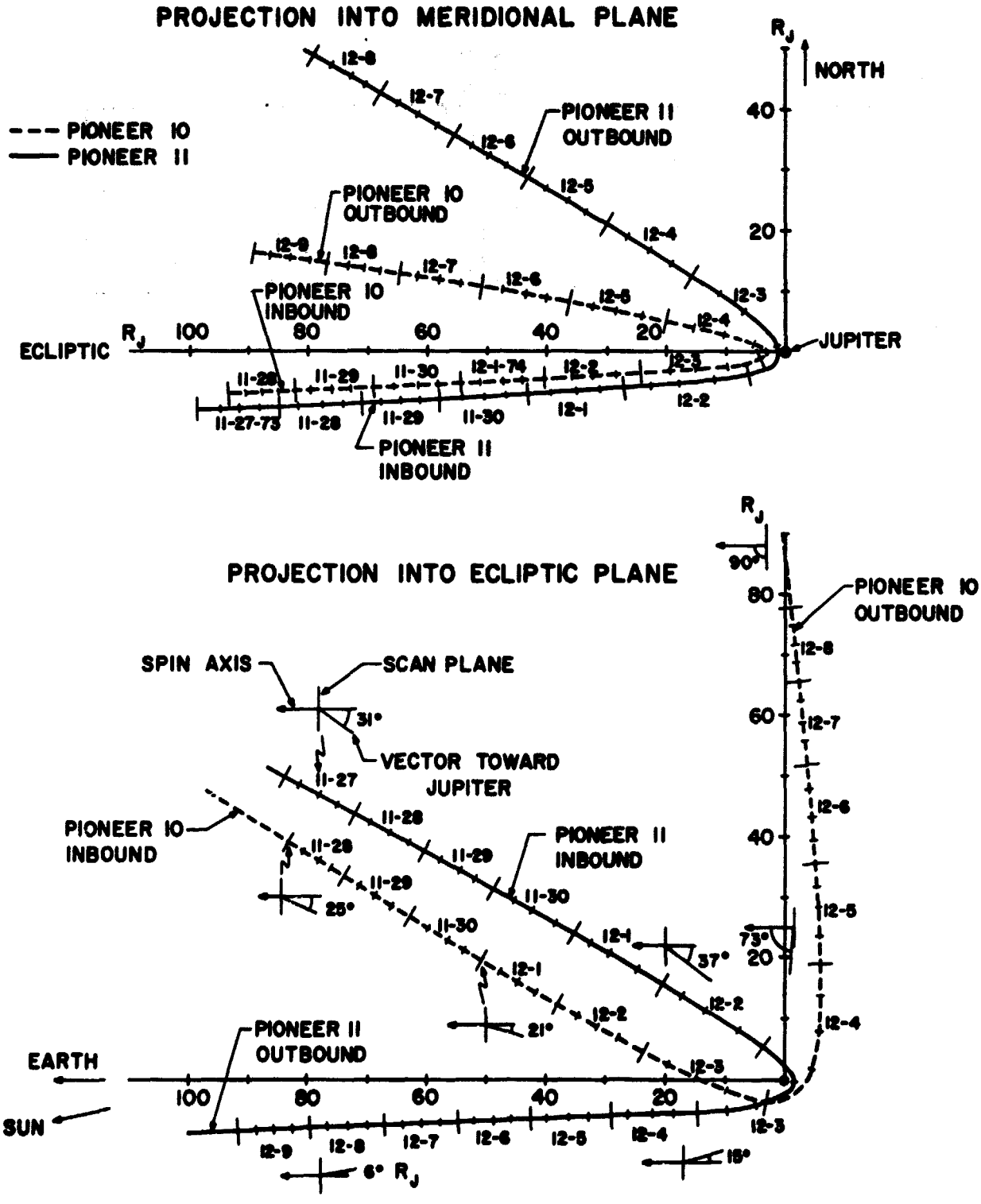
PROJECTION INTO MERIDIONAL PLANE
PIONEER 10
PIONEER 11
PIONEER 11 OUTBOUND
PIONEER 10 OUTBOUND
PIONEER 10 INBOUND
PIONEER 11 INBOUND
NORTH
ECLIPTIC
JUPITER
PROJECTION INTO ECLIPTIC PLANE
SPIN AXIS
SCAN PLANE
VECTOR TOWARD JUPITER
EARTH
SUN

Fig. 1

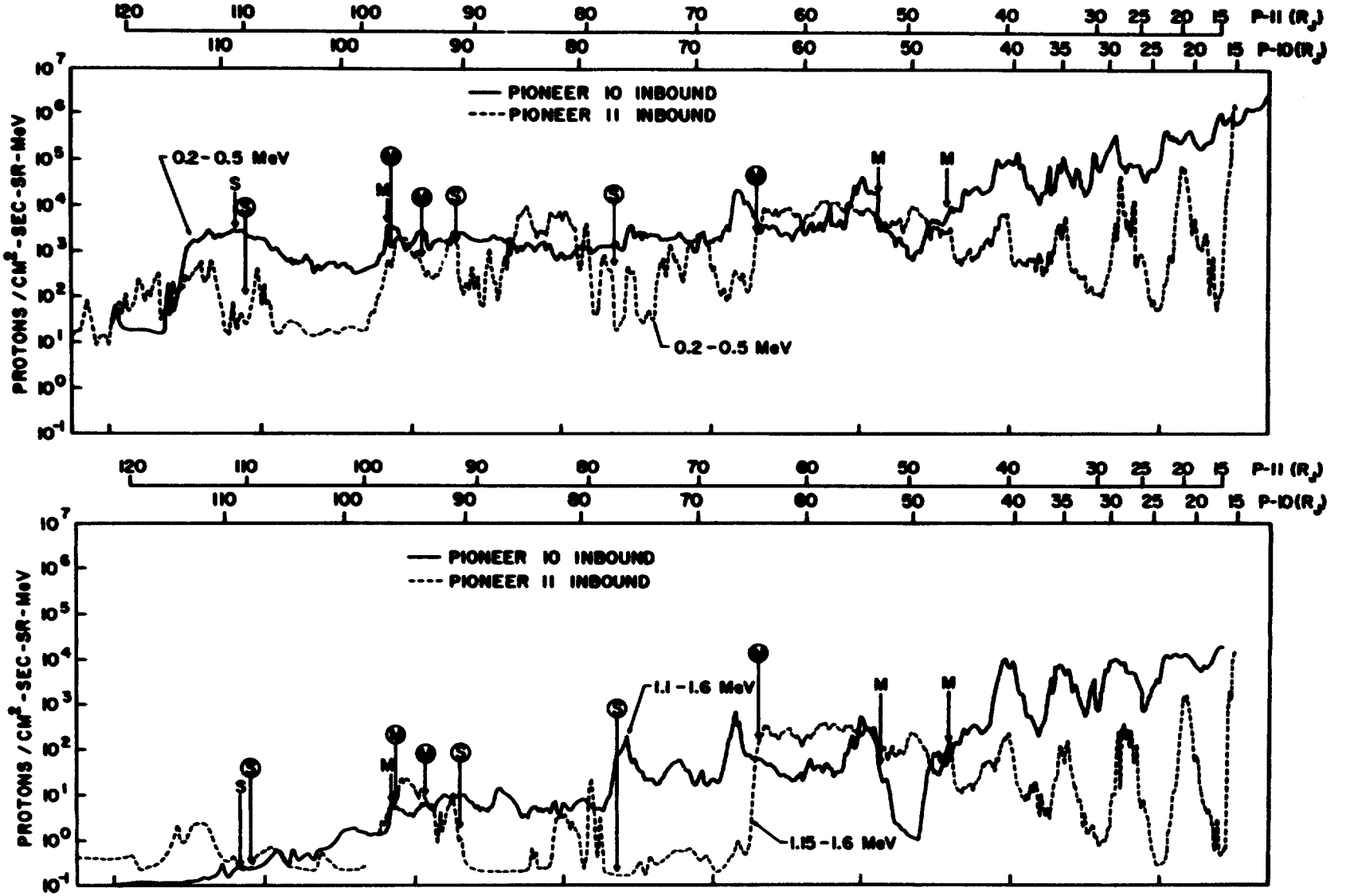
P-11 (R_J)
P-10(R_J)
PIONEER 10 INBOUND
PIONEER 11 INBOUND
0.2-0.5 MeV
PROTONS / CM²-SEC-SR-MeV
1.1-1.6 MeV
1.15-1.6 MeV

Fig. 2

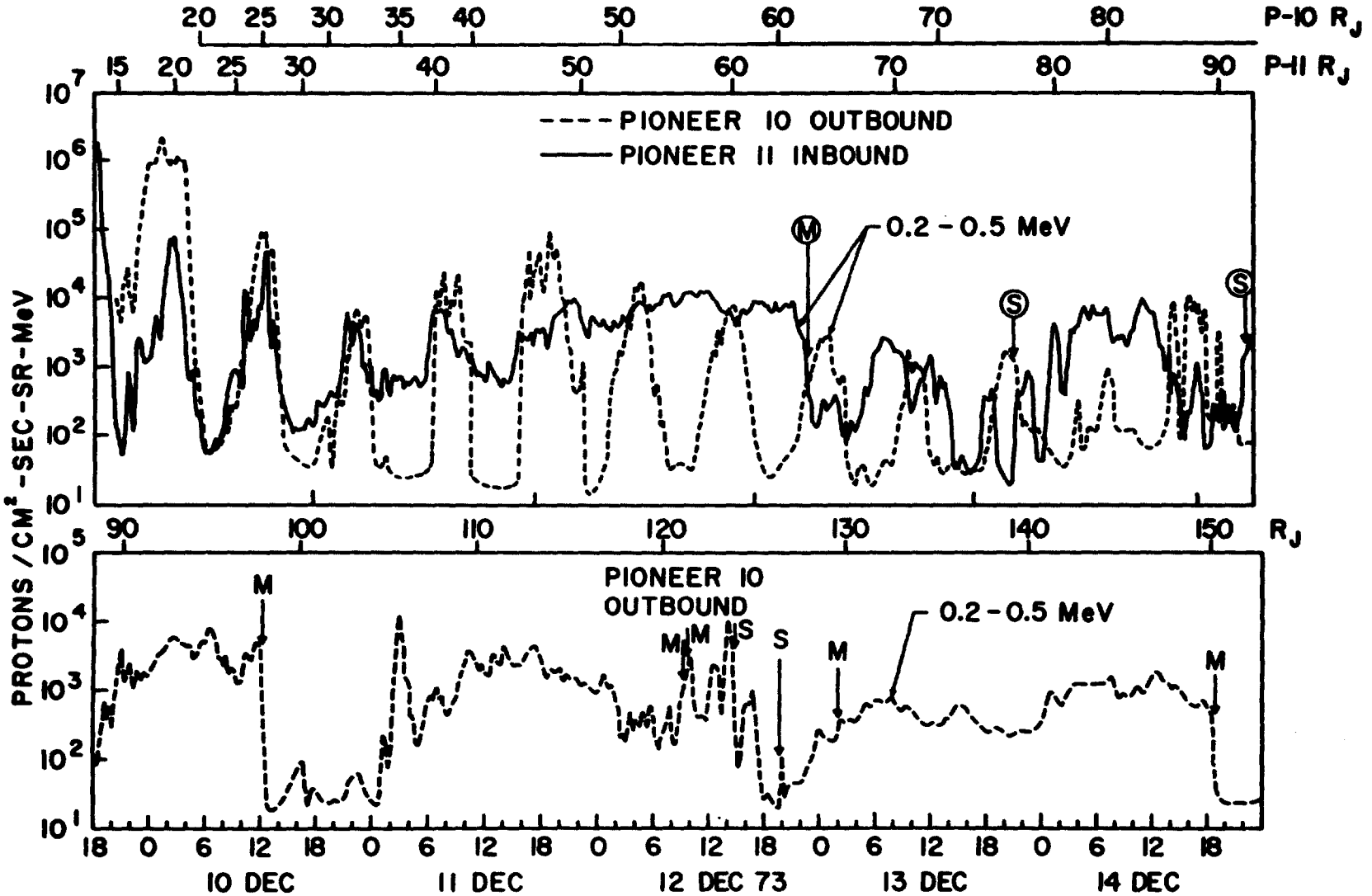

Fig. 3

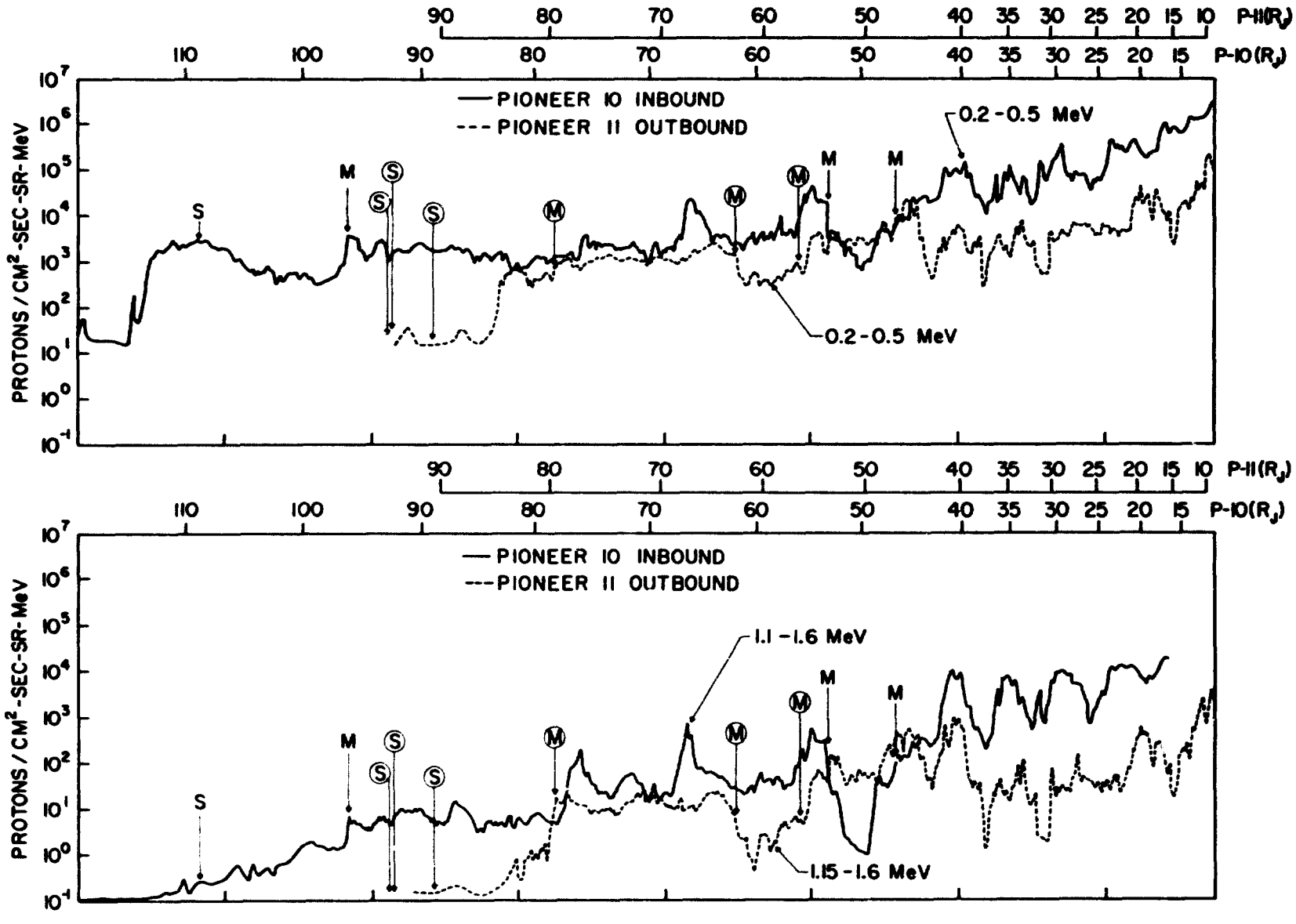
P-11(R_J)
P-10(R_J)
PIONEER 10 INBOUND
PIONEER 11 OUTBOUND
0.2 - 0.5 MeV
PROTONS / CM² - SEC - SR - MeV
1.1 - 1.6 MeV
1.15 - 1.6 MeV
S
M

Fig. 4

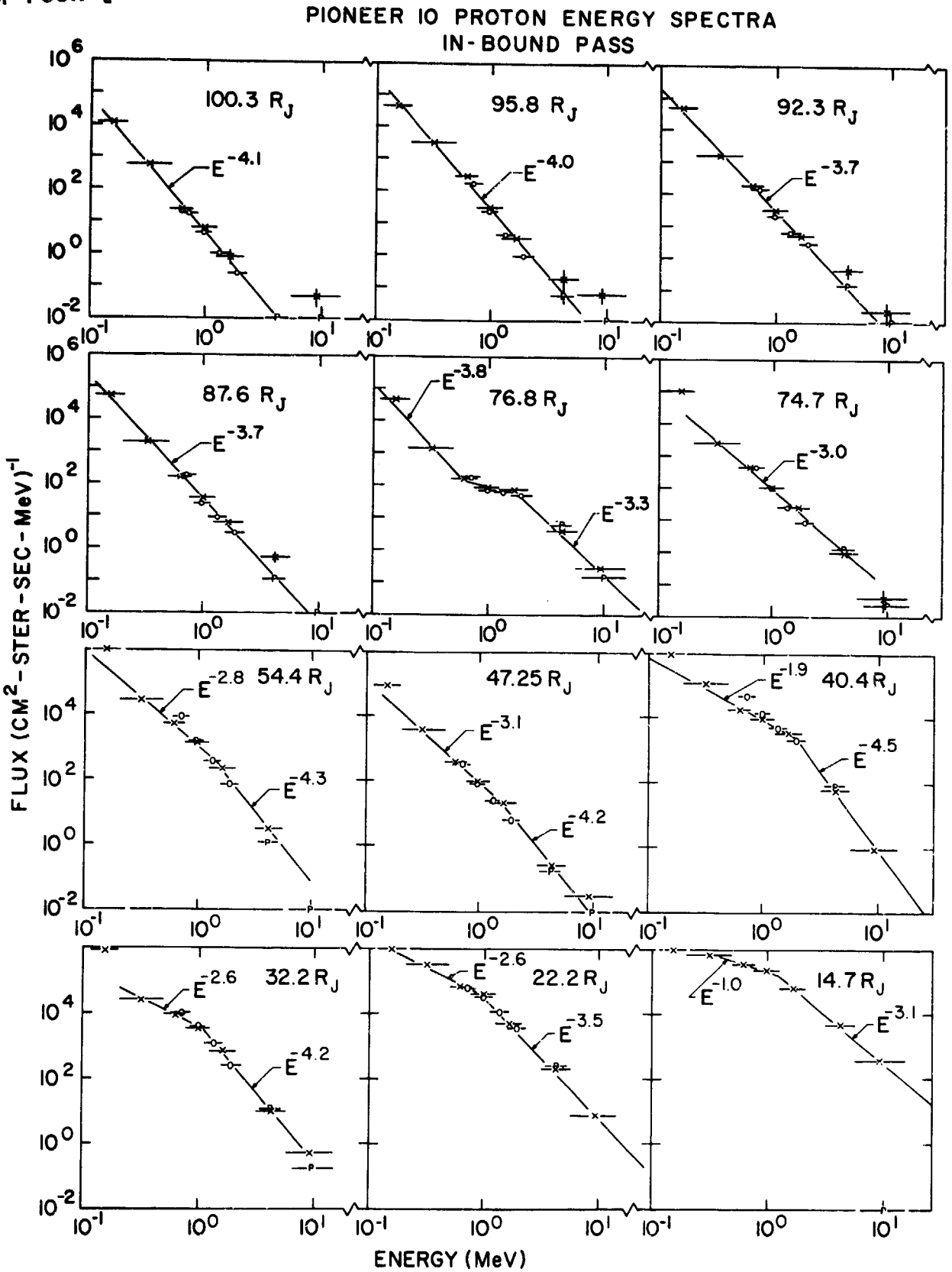

Fig. 5

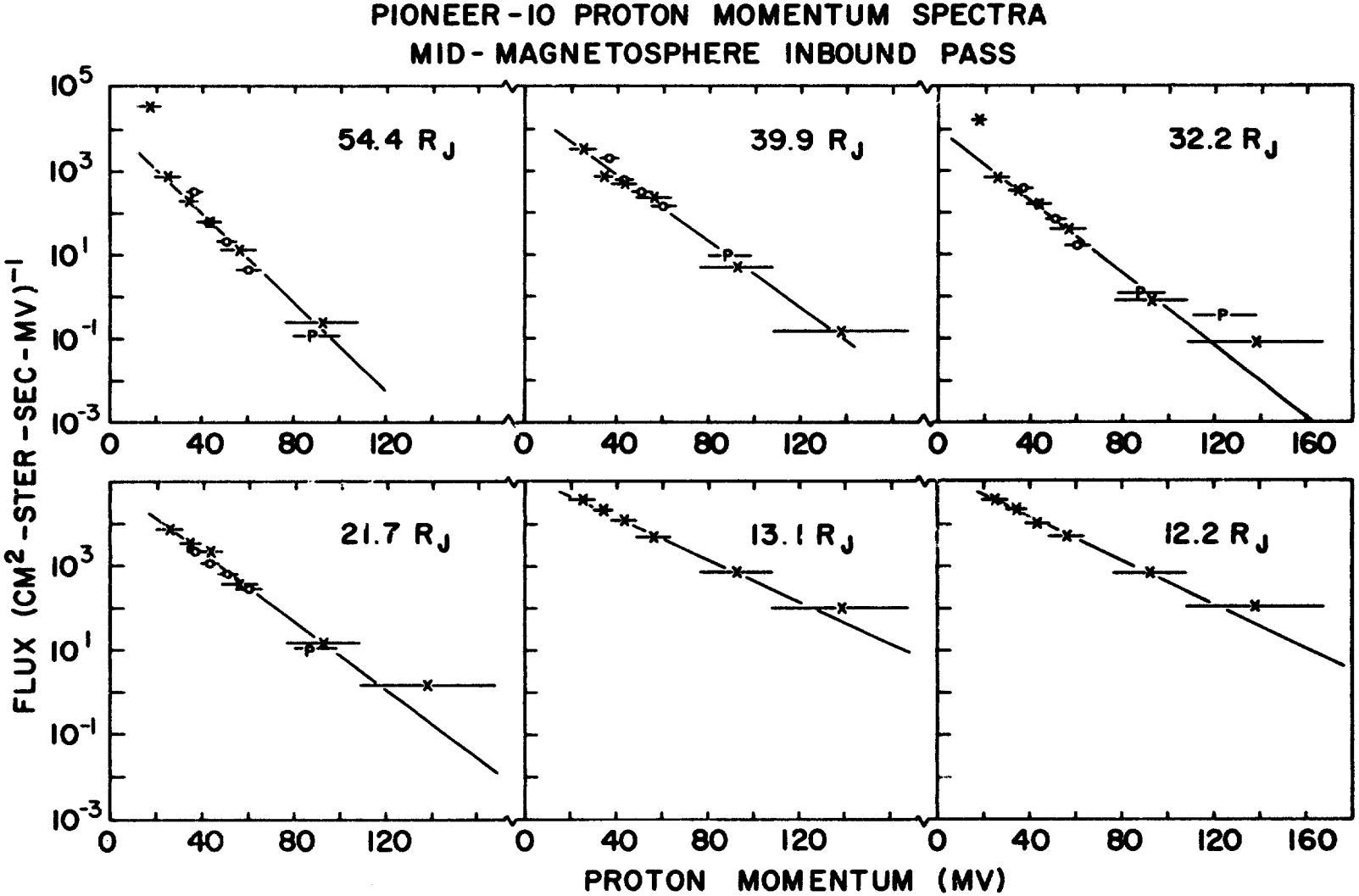
PIONEER-10 PROTON MOMENTUM SPECTRA
MID-MAGNETOSPHERE INBOUND PASS
54.4 R_J
39.9 R_J
32.2 R_J
21.7 R_J
13.1 R_J
12.2 R_J
FLUX (CM²-STER-SEC-MV)⁻¹
PROTON MOMENTUM (MV)

Fig. 6

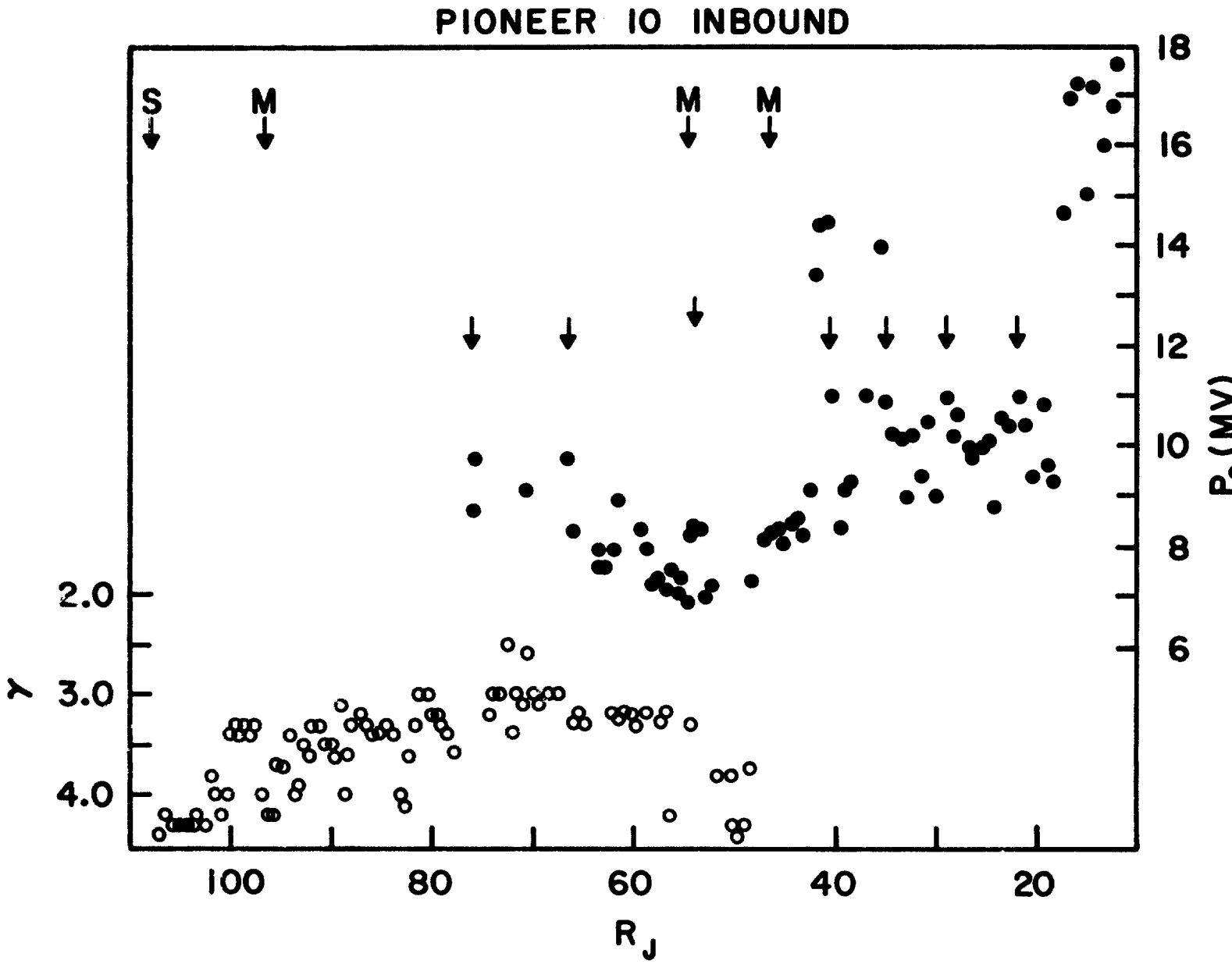
PIONEER 10 INBOUND
S
M
M
M
18
16
14
12
10
8
6
2.0
3.0
4.0
γ
100
80
60
40
20
R_J
P_e (MV)

Fig. 7

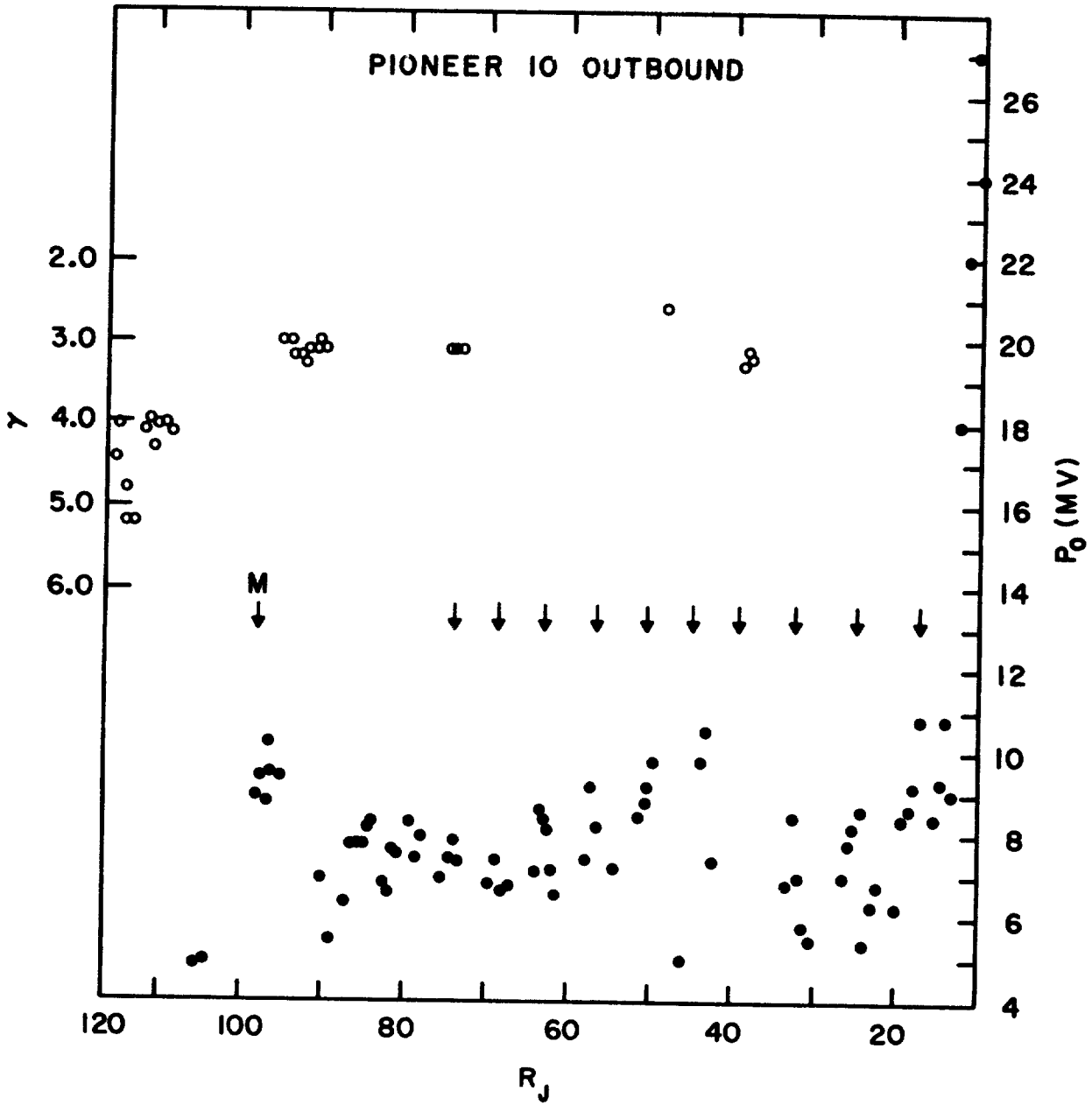
PIONEER 10 OUTBOUND
2.0
3.0
4.0
5.0
6.0
γ
M
26
24
22
20
18
16
14
12
10
8
6
4
P_0 (MV)
120
100
80
60
40
20
R_J

Fig.8

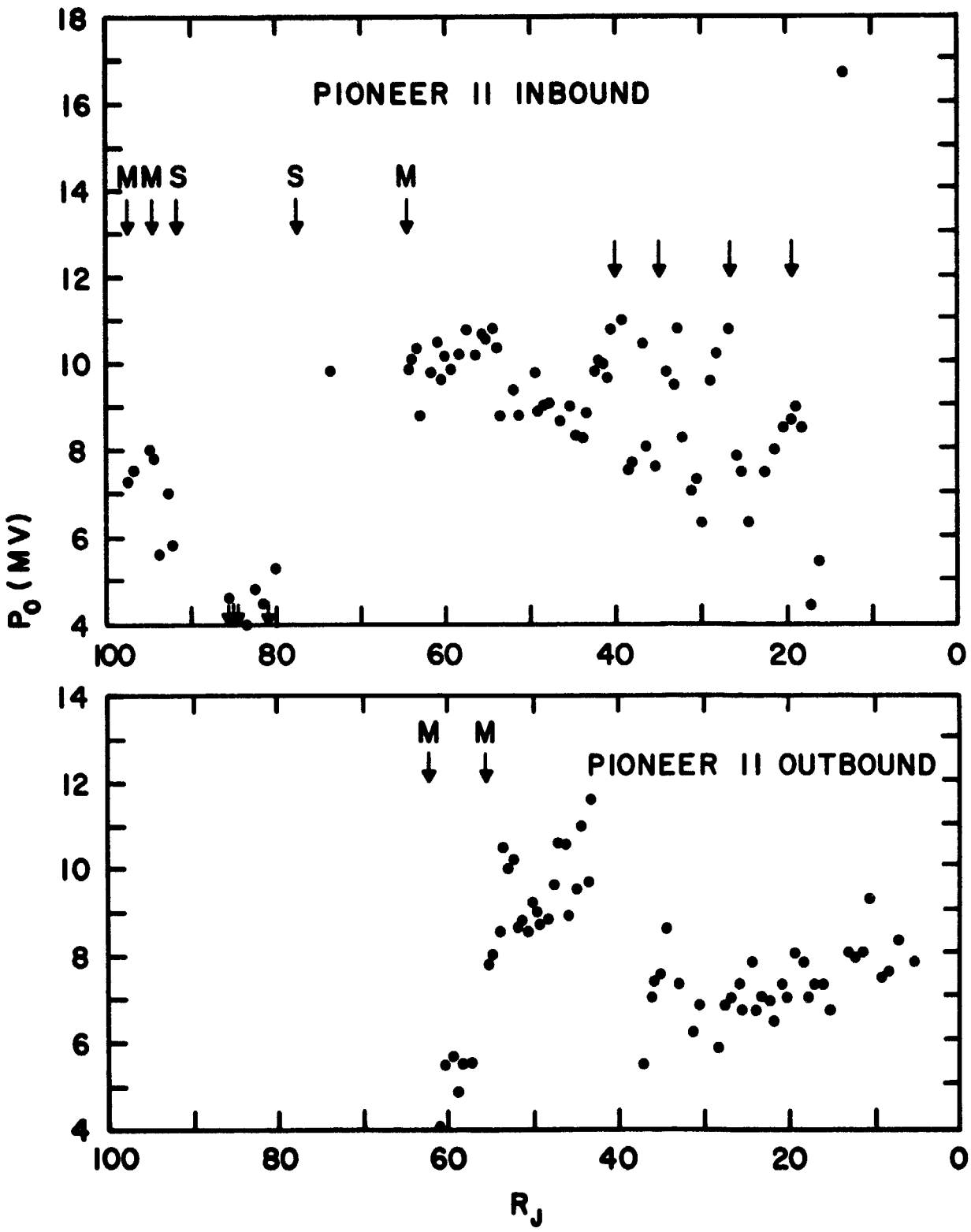
PIONEER II INBOUND
MMS
S
M
P_0 (MV)
18
16
14
12
10
8
6
4
100
80
60
40
20
0
PIONEER II OUTBOUND
M
M
14
12
10
8
6
4
100
80
60
40
20
0
R_J

Fig. 9

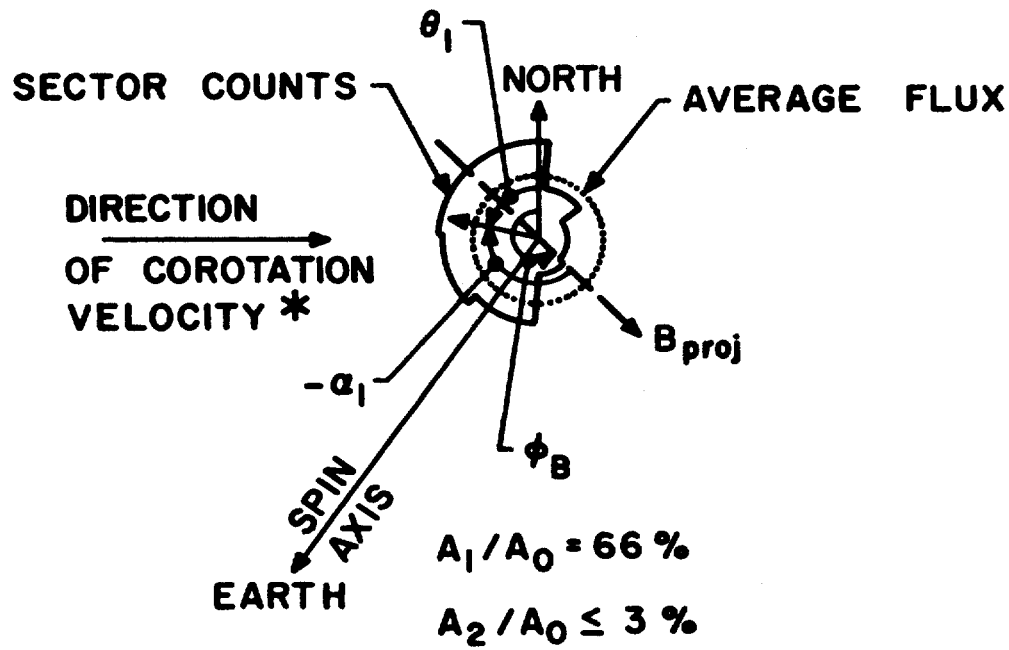
θ_1
SECTOR COUNTS
NORTH
AVERAGE FLUX
DIRECTION
OF COROTATION
VELOCITY *
B_{proj}
$-\alpha_1$
ϕ_B
SPIN AXIS
EARTH
$A_1/A_0 = 66\ \%$
$A_2/A_0 \leq 3\ \%$
* EXCEPT ON P-10 OUT

Fig. 10

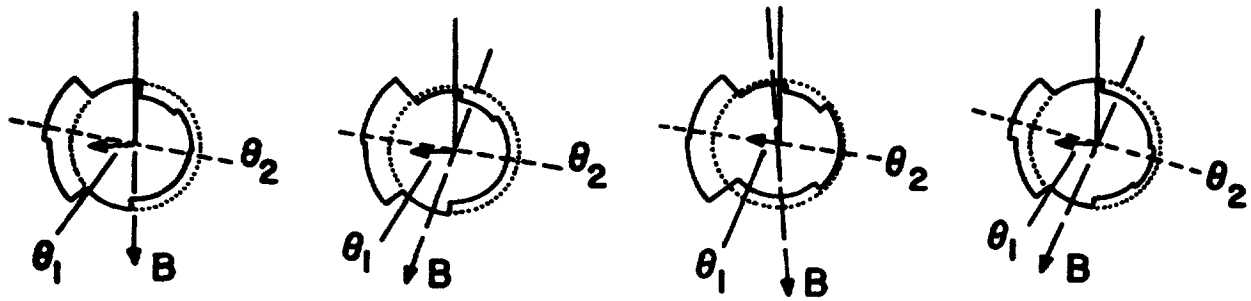

FLUX MAXIMA

$a_1 = 28\%$ $a_2 = 14\%$ 22:00 1 DEC '73 A

$a_1 = 28\%$ $a_2 = 15\%$ 7:00 2 DEC '73 B

$a_1 = 23\%$ $a_2 = 23\%$ 16:00 2 DEC '73 C

$a_1 = 24\%$ $a_2 = 13\%$ 3:00 3 DEC '73 D

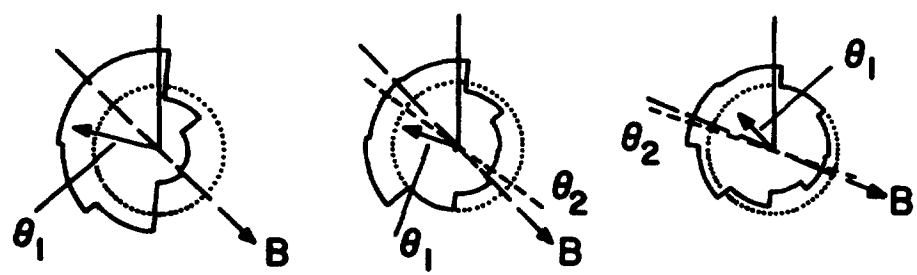

FLUX MINIMA

$a_1 = 66\%$ $a_2 \leq 3\%$ 3:00 2 DEC '73 AB

$a_1 = 45\%$ $a_2 \leq 5\%$ 12:00 2 DEC '73 BC

$a_1 = 32\%$ $a_2 = 7\%$ 21:00 2 DEC '73 CD

PIONEER 10 INBOUND , 1.8 – 2.15 MeV PROTONS

Fig. 11

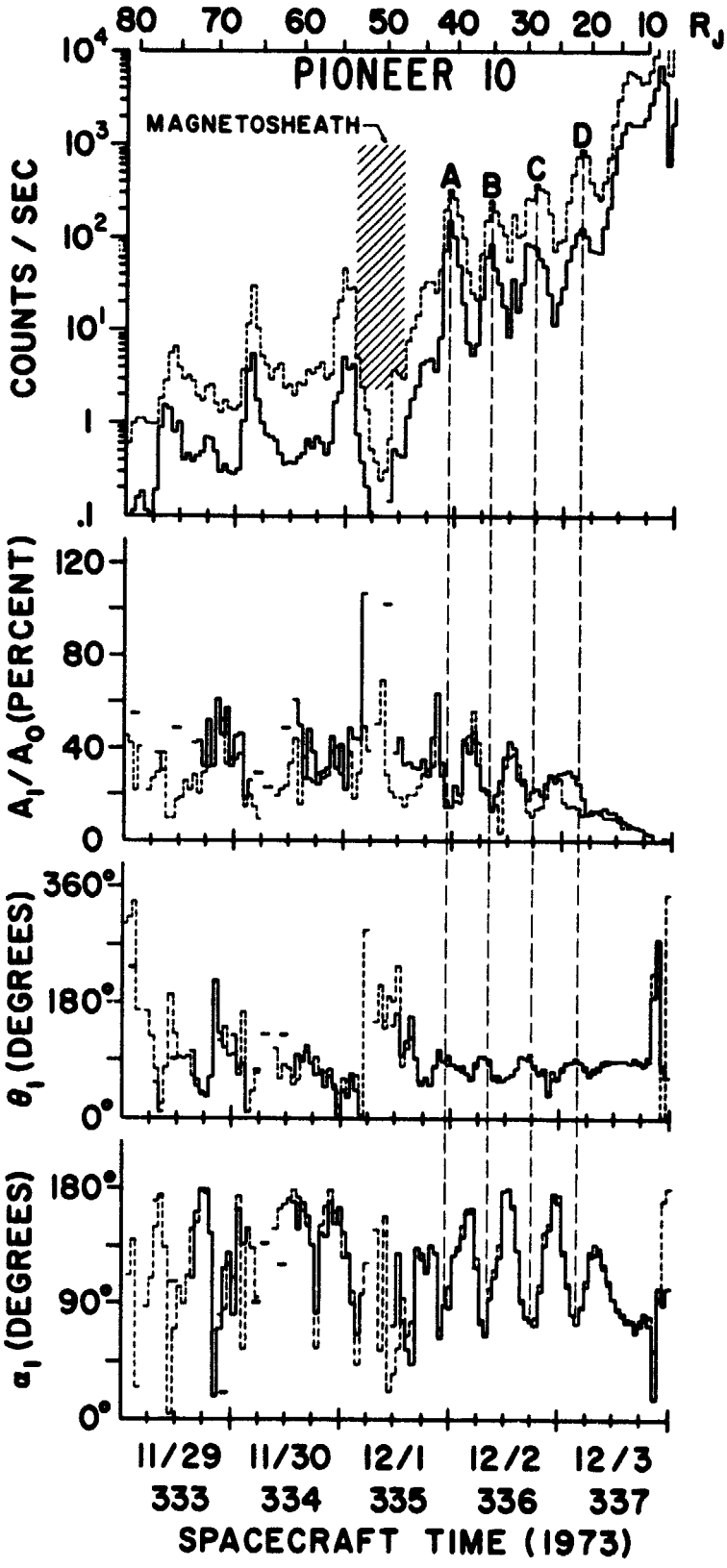

Fig. 12

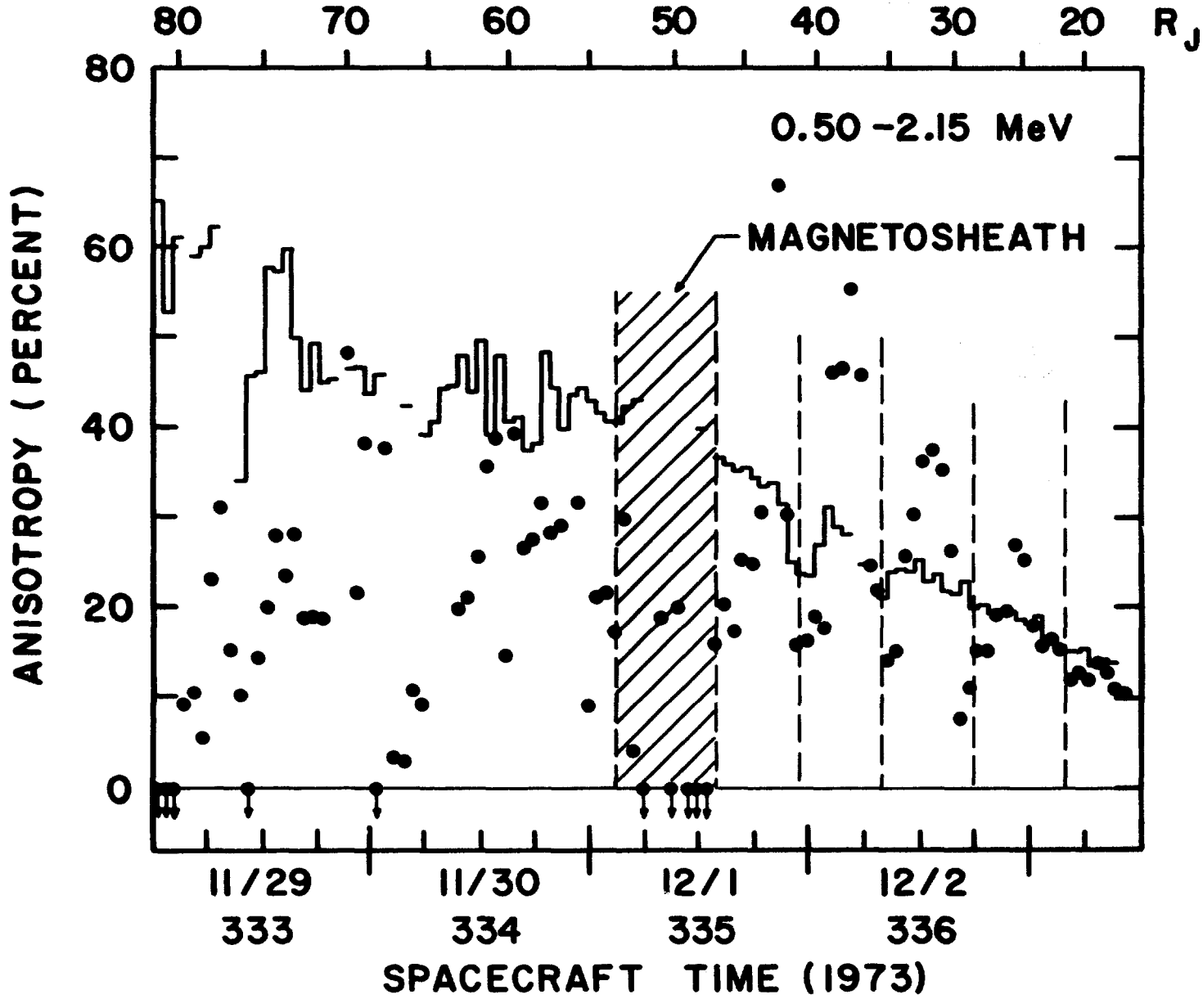
80
70
60
50
40
30
20
R_J
0.50 -2.15 MeV
MAGNETOSHEATH
ANISOTROPY (PERCENT)
80
60
40
20
0
11/29
333
11/30
334
12/1
335
12/2
336
SPACECRAFT TIME (1973)

Fig. 13

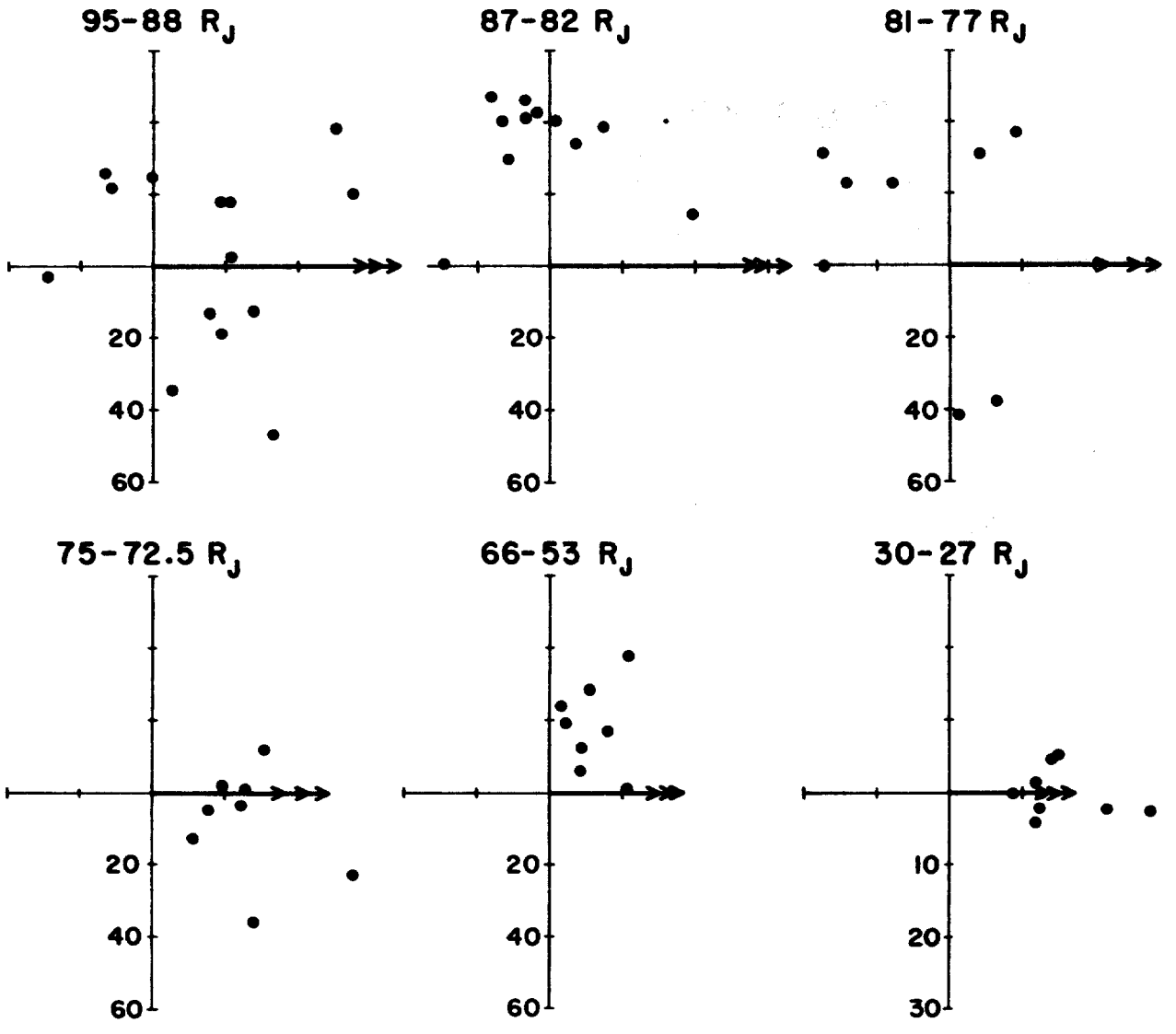

MEASURED PIONEER 10 ANISOTROPIES A_1/A_0 vs. θ_1
0.5-2.2 MeV PROTONS INBOUND PASS

Fig. 14

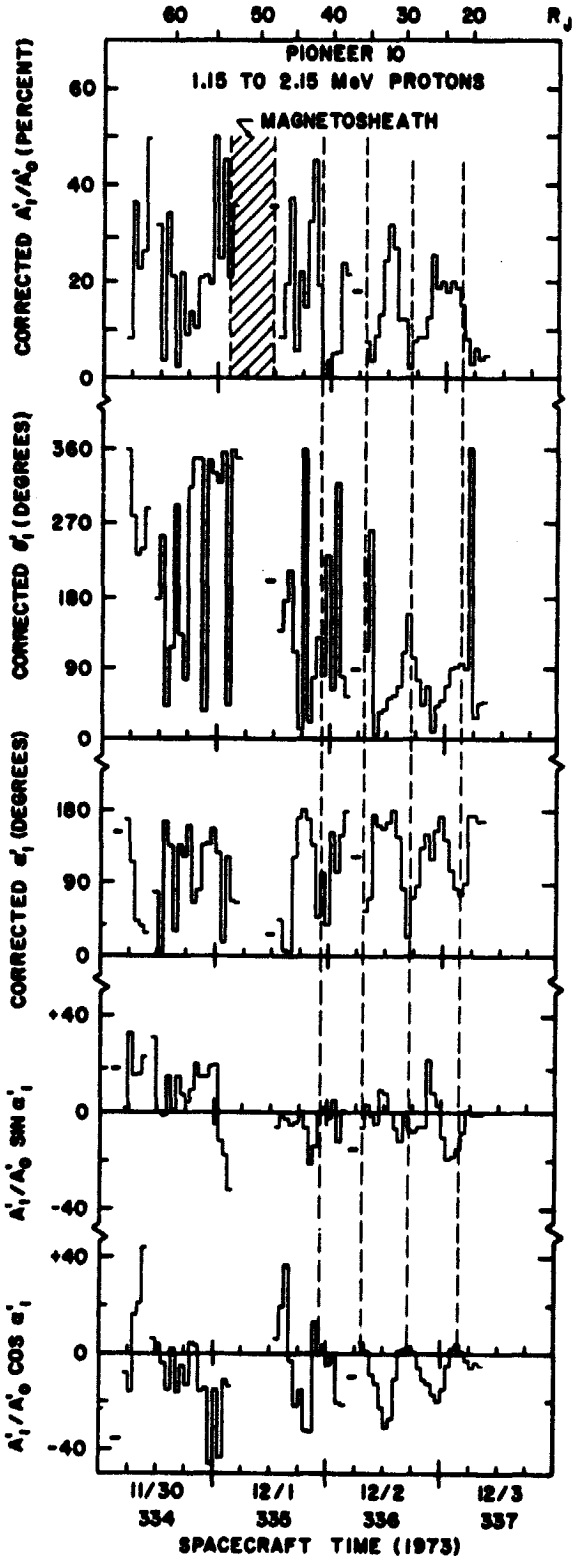

Fig. 15

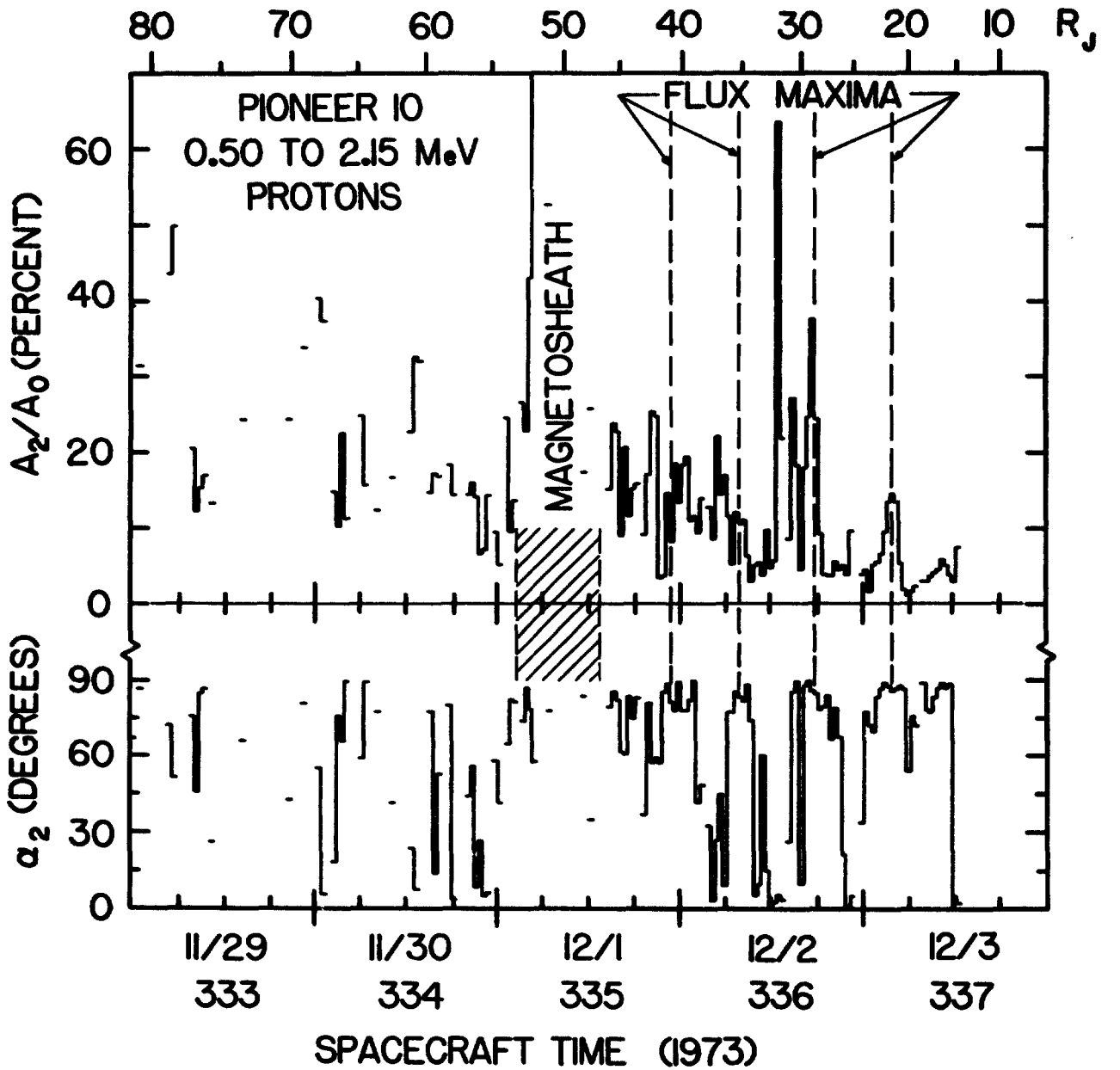

Fig. 16

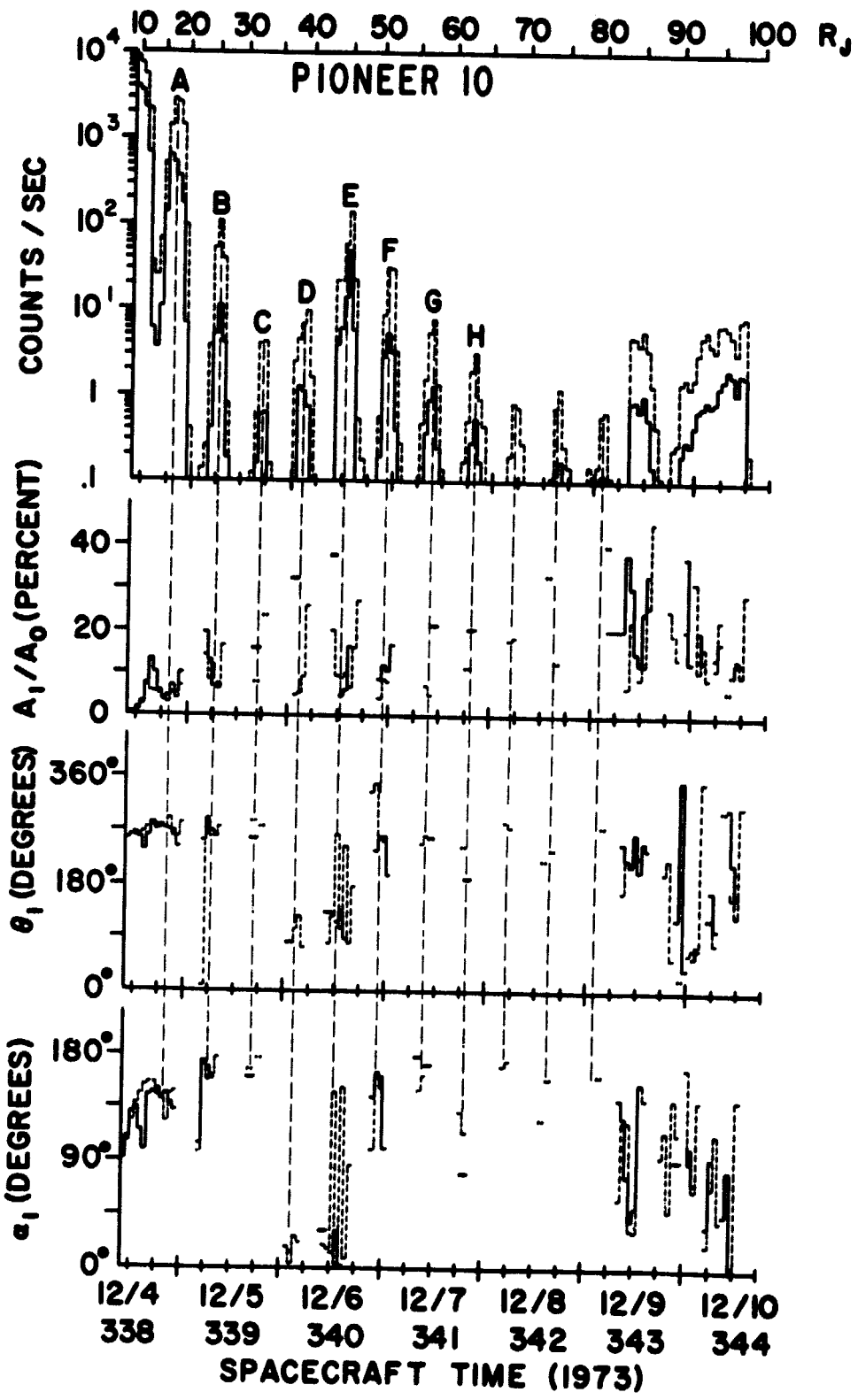

Fig. 17

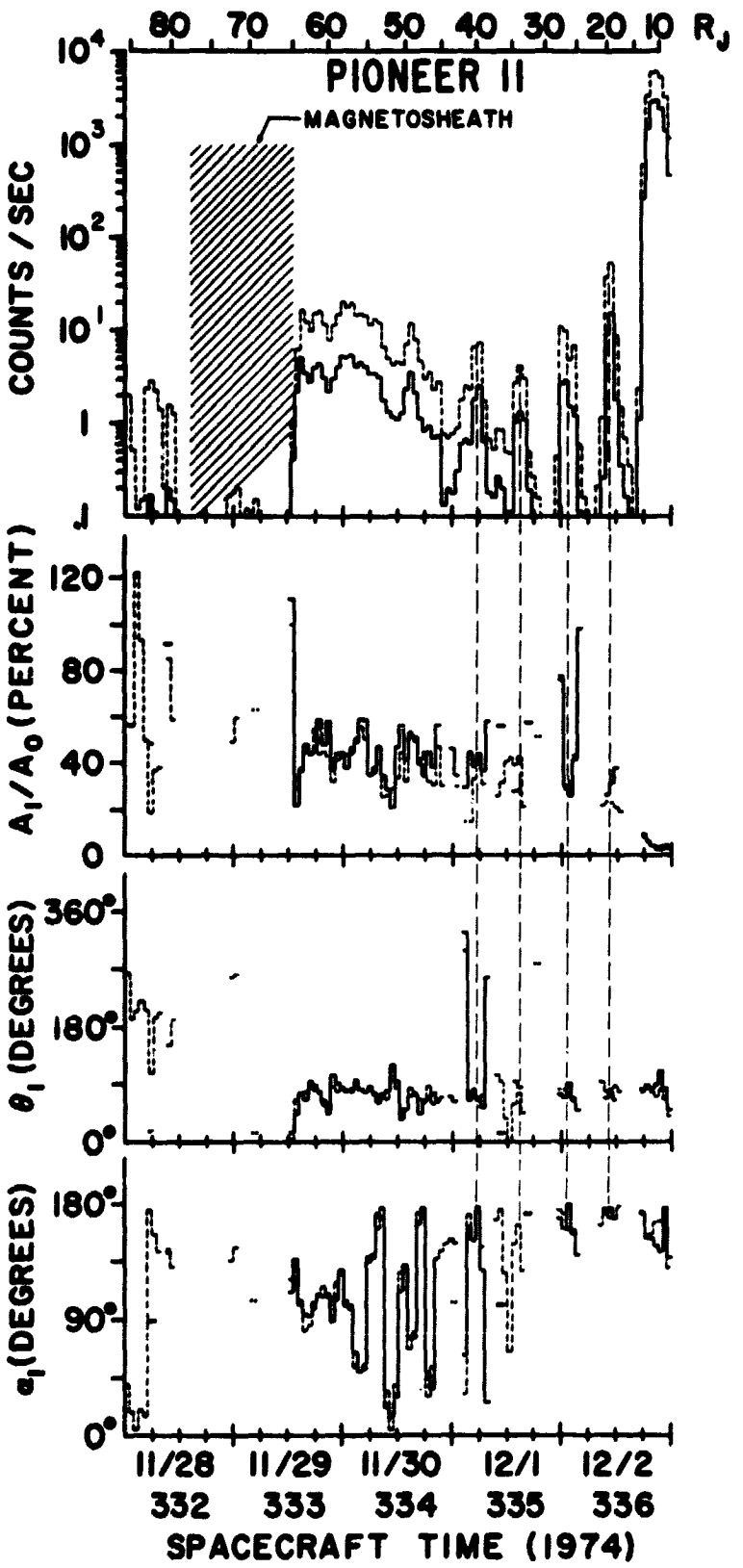
80 70 60 50 40 30 20 10 R_J
PIONEER 11
MAGNETOSHEATH
COUNTS / SEC
10^4
10^3
10^2
10^1
1
A_1/A_0 (PERCENT)
120
80
40
0
θ_1 (DEGREES)
360°
180°
0°
α_1 (DEGREES)
180°
90°
0°
11/28
332
11/29
333
11/30
334
12/1
335
12/2
336
SPACECRAFT TIME (1974)

Fig. 18

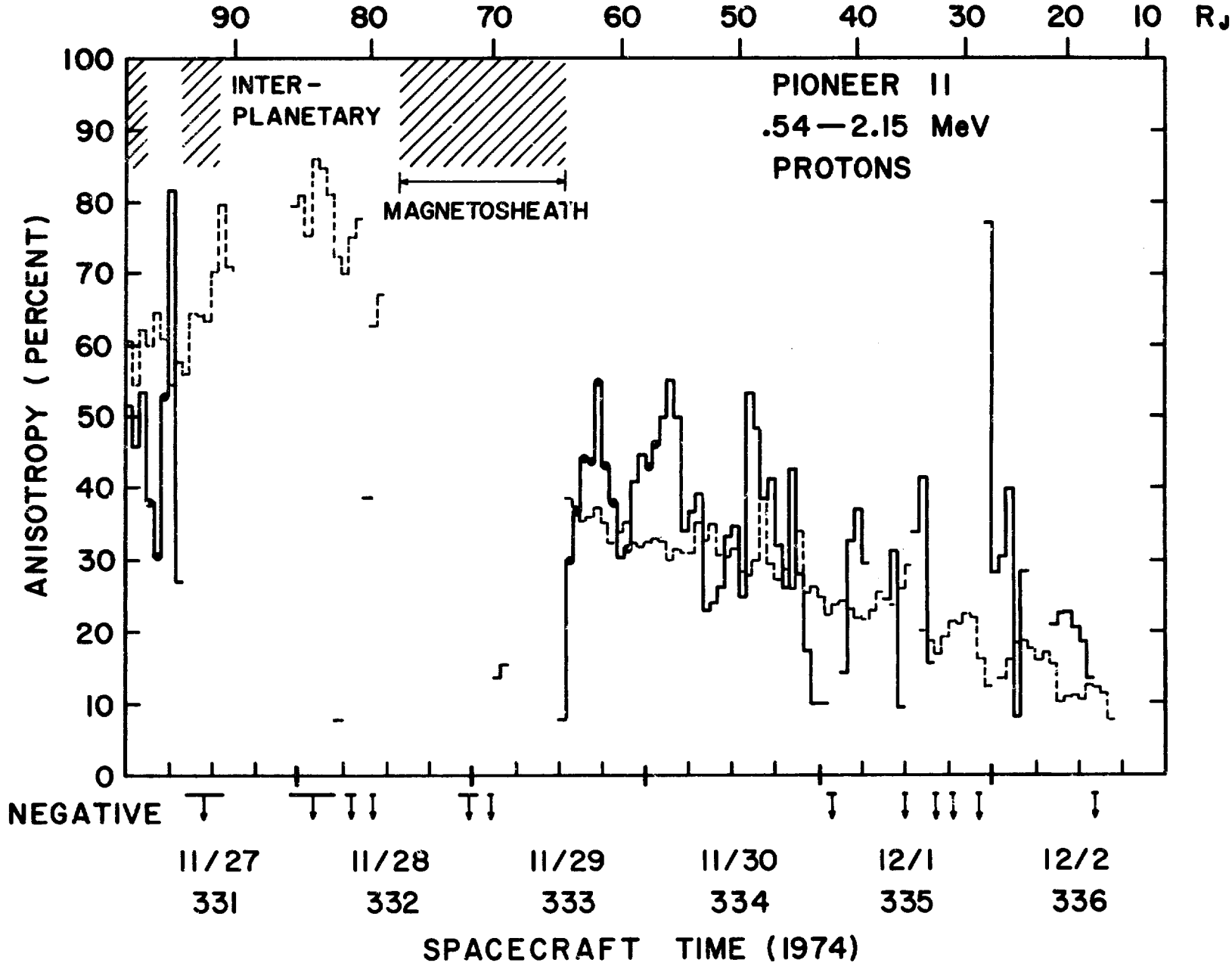

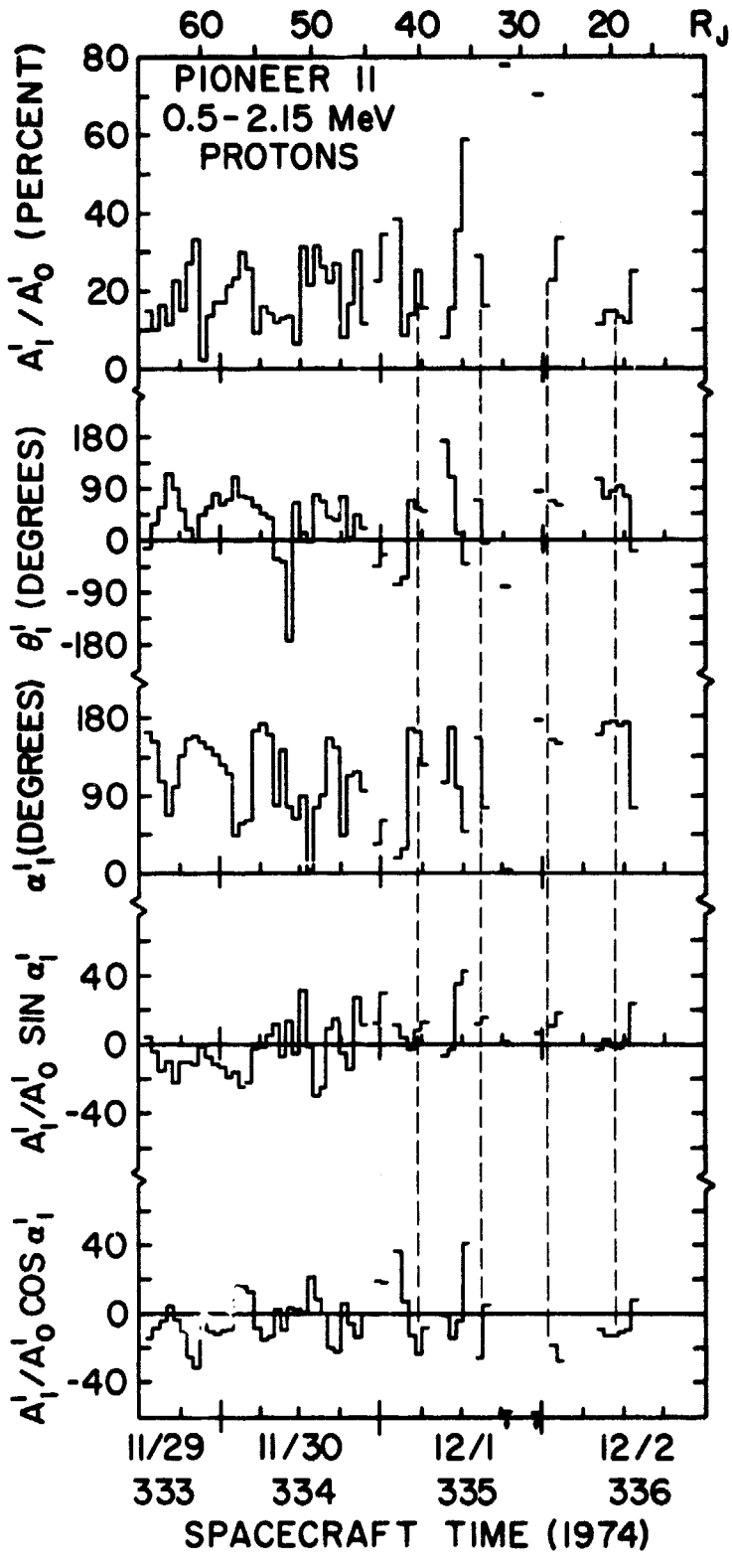
60
50
40
30
20
R_J
PIONEER II
0.5-2.15 MeV
PROTONS
A_1'/A_0' (PERCENT)
80
60
40
20
0
θ_1' (DEGREES)
180
90
0
-90
-180
α_1' (DEGREES)
180
90
0
A_1'/A_0' SIN α_1'
40
0
-40
A_1'/A_0' COS α_1'
40
0
-40
11/29
333
11/30
334
12/1
335
12/2
336
SPACECRAFT TIME (1974)

Fig. 20

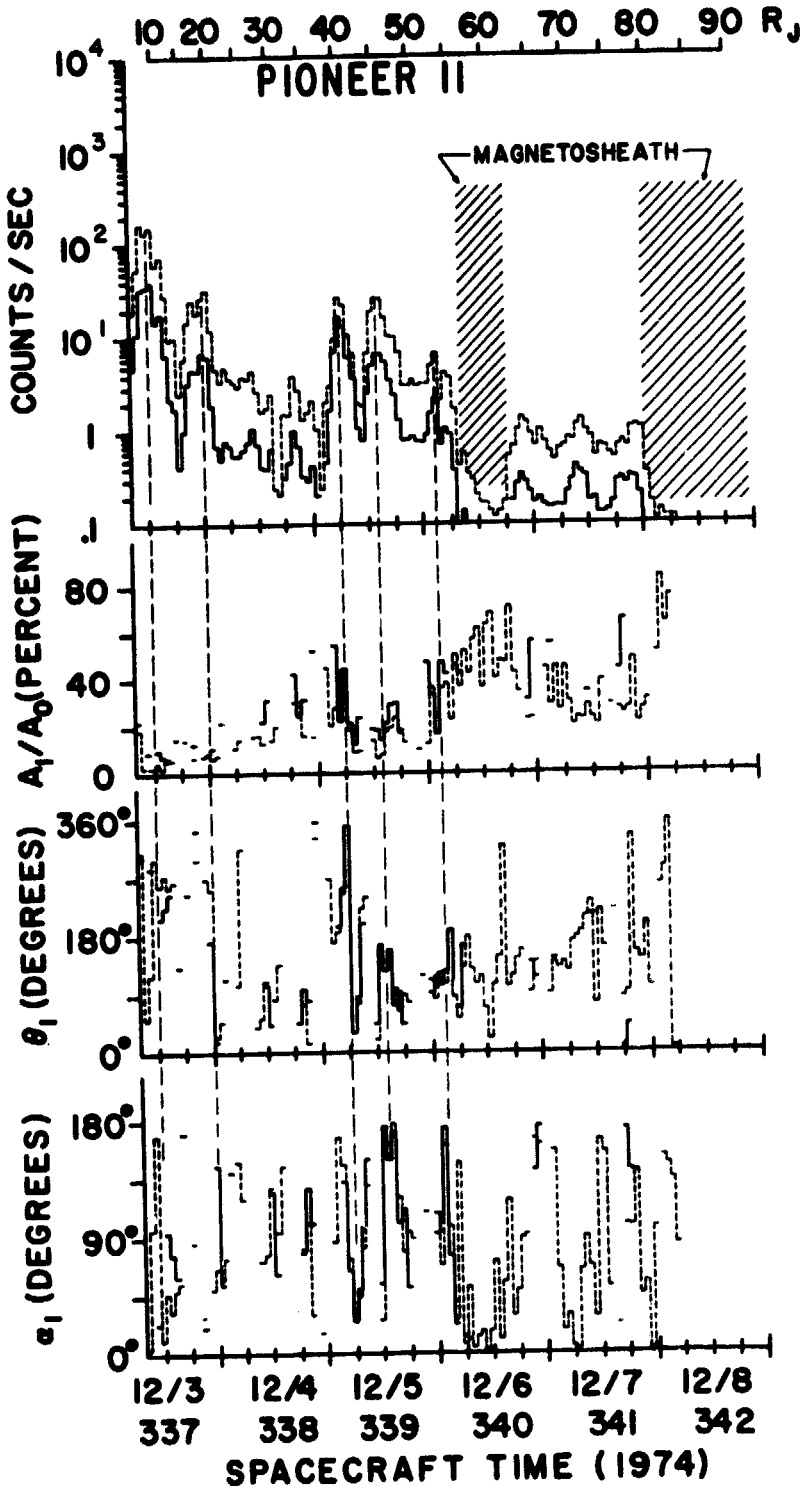

Fig. 21

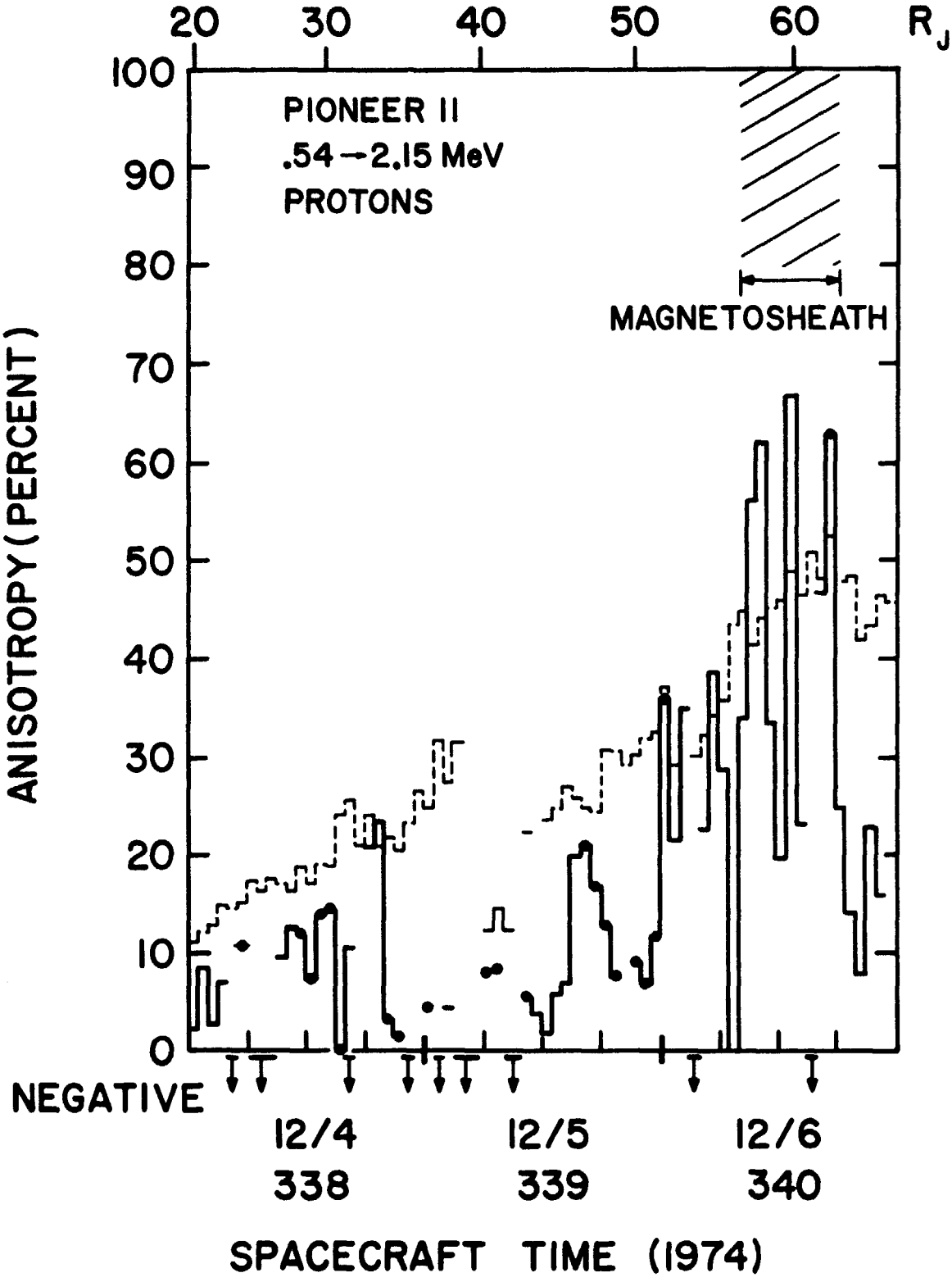
20
30
40
50
60
R_J
100
90
80
70
60
50
40
30
20
10
0
PIONEER II
.54 – 2.15 MeV
PROTONS
MAGNETOSHEATH
ANISOTROPY (PERCENT)
NEGATIVE
12/4
338
12/5
339
12/6
340
SPACECRAFT TIME (1974)

Fig.22

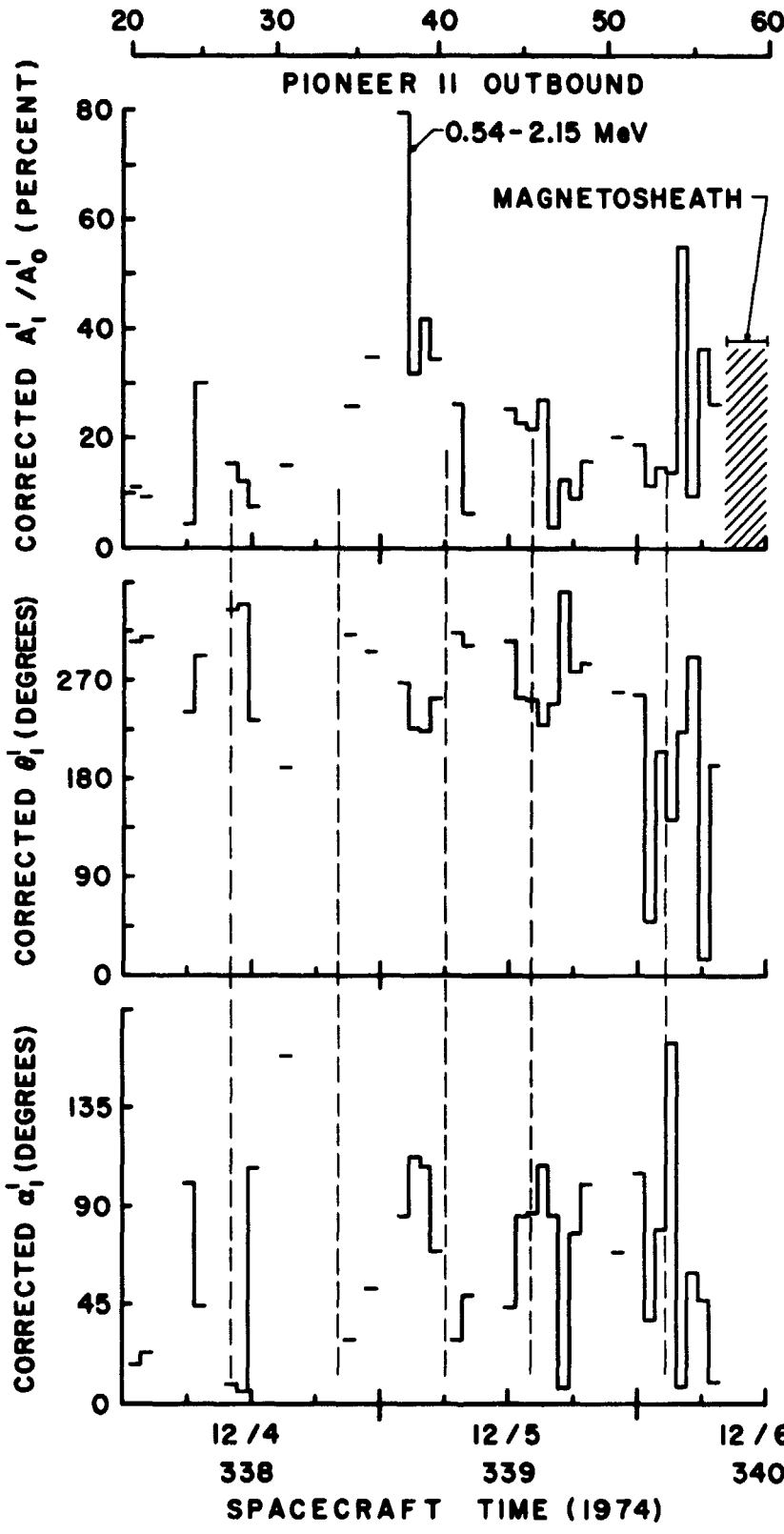

ORIGINAL PAGE IS
OF POOR QUALITY

Fig.23